UNIVERSITY OF CALIFORNIA, SAND DIEGO

SYNTHESIS OF NICKEL-ALUMINUM METAL-INTERMETALLIC-LAMINATE COMPOSITES

A Thesis submitted in partial satisfaction of the requirements for the degree
Master of Science

in

NanoEngineering

by

Xin Liu

Committee in Charge:

Professor Kenneth S. Vecchio
Professor Vlado Lubarda
Professor Jian Luo

2014

The Thesis of Xin Liu is approved, and it is acceptable in quality and form for publication on microfilm and electronically:

_____

_____

_____

Chair

University of California, San Diego

2014

DEDICATION

In recognition of the guidance he has provided over the past two years, this thesis is dedicated to my advisor, Dr. Kenneth Vecchio.

Additionally, this thesis is dedicated to my parents, Junyou Liu and Weiqun Ren, and brother Chang Liu for their support and understanding.

TABLE OF CONTENTS

LIST OF ABBREVIATIONS

MIL composite: Metal-intermetallic-laminate composite

XRD: X-ray diffractometer

BCC: Body centered cubic

FCC: Face centered cubic

SEM: Scanning electron microscope

EDS: Energy dispersive spectroscopy

SE: Secondary electron

BSE: Back-scatter electron

LIST OF FIGURES

LIST OF GRAPHS

LIST OF TABLES

ACKNOWLEDGEMENT

I would like to acknowledge Professor Kenneth S. Vecchio for his guidance and support as the chair of my committee in the past two years, from who I learned not only the meaning of dedication but also the importance of enthusiasm on the things that one does.

I would also like to thank Mr. Wayne Neilson, our lab technician and my sincere friend. I also owe gratitude to Sabine Faulhaber and Yu Wang for their help and support.

ABSTRACT OF THE THESIS

SYNTHESIS OF NICKEL-ALUMIMUM METAL-INTERMETALLIC-LAMINATE COMPOSITES

By

Xin Liu

Master of Science in NanoEngineering

University of California, San Diego, 2014

Professor Kenneth S. Vecchio

As pointed out by the in-depths studies on the mechanical and physical properties, intermetallic compounds have shown great potentials for applications in both structural and non-structural fields at elevated temperatures. [1] In spite of their high melting

temperature, low density and excellent corrosion and oxidation resistance exhibited under extreme environments, unfortunately, many intermetallic materials are brittle at room temperature. Such brittleness in most cases limits the fabrication and processing for structural applications. [2] To eliminate or alleviate the influence of brittleness and further utilize intermetallics in industries, methods like alloying and coating, have been intensively studied on several typical intermetallics such as FeAl, Fe_3Al, and Ni_3Al. [3, 4] In the present study, the method of metal-intermetallic laminate composites synthesis [5, 6] was used as the approach to increase the overall ductility via combining constituent metals and intermetallics. Three systems were studied, including the binary nickel-aluminum reaction system, the ternary system on synthesis reactions between aluminum and nickel-chromium alloy, and the quaternary system using aluminum and nickel-iron-chromium alloy. A standard processing profile was used for complete reaction on all systems. To investigate the reaction evolution, the method of reaction interruption was used to study the microstructure evolution at different stages of the reactions in the systems. For Ni-Al system, MIL composites of Ni-(Al_3Ni_2+Al_3Ni) and Ni-Al_3Ni_2 were fabricated. For Ni-Fe-Al system, MIL composites synthesizing with Invar and aluminum, intermetallic phases of $Al_{79}Fe_{16}Ni_6$ and $Al_{84}Fe_9Ni_7$ were obtained. And for Ni-Cr-Fe-Al systems using Inconel and aluminum, intermetallic phases of $Al_{80}Cr_3Fe_3Ni_7Mo$ and $Al_{85}Cr_3Fe_3Ni_7Mo$ were found.

CHAPTER 1: INTRODUCTION

Intermetallic materials, as a bridge connecting between metallic and non-metallic materials, have unique physical and mechanical properties. Yet the rigid structure of intermetallics leads to brittleness which makes it hard to process. To minimize the impact of the drawbacks, intermetallics can be fabricated into composite material. Composite materials are a genre of materials that consist of two or more component materials, which have distinctive physical and chemical properties. Such kind of combination is aimed to utilize excellent properties of each of the individual component materials, circumvent drawbacks such as brittleness that the individual components may possess, and obtain an improved overall performance in the final composite product, for instance, a stronger and lighter composite comparing to the individual component parts. The superior properties of a composite comparing to those of the components have always been the goal to achieve in materials design. Since it is possible to achieve a highly customizable product for specific industrial purposes, composite materials are widely used in various fields and industries. The application of composite materials can range from bricks made of straw and mud for building construction in Ancient Egypt and laminate composites used for fuselage and wings in aircraft. Composites made of continuous fibers are widely used for high structural performance. Also, from a cost-effective perspective, composites are a good candidate to replace expensive component materials. Examples of widely used composite materials in daily life include ceramic composites, metal composites, and reinforced plastics. Among different types of composite materials, laminated metal composites present significant improvement in properties such as fracture toughness, corrosion and fatigue behavior.

As the demand for property improvements in engineering materials often exceed those achieved via conventional processing methods, one way to process novel materials is the application of laminated composites. Aluminum and its alloys, for the ease of handling and cost-effective properties like light weight, are often selected in new processes for novel materials research in the advanced aerospace and aircraft industries.

Laminates produced using alternating layers of aluminum sheets and other materials like plies of fibers have notably improved resistance to crack propagation. Commonly applied examples are ARALL and GLARE (GLAss REinforced laminate). ARALL composites may have a tensile stress as high as 800 MPa and an elongation of 2.5%, comparing to 570 MPa and 11% for aluminum 7075-T6, an aluminum alloy containing small traces of Cr (0.18 - 0.28wt.%), Cu, Fe, Mg, Ti and other elements. While ARALL and 7075-T6 have comparable elastic modulus, yet the former has a lower density. As ARALL was developed mainly for applications in aircraft wings, GLARE may be used for upper fuselage in Airbus A380. GLARE is made of alternating layers of aluminum sheets and continuous meshes of glass fibers in an epoxy resin adhesive. By adjusting the parameters like ratio in fiber-resin system, alloy type, layer thickness, and stacking sequence and so on, the laminate may be customized to meet certain requirements. [7]

Similar to the laminated composites mentioned above, laminated metal composites comprising alternating layers of different metal or metal-containing phases have shown that the many properties including fracture toughness, corrosion and ductility can be enhanced via the lamination method. Recently, as a new branch of structural materials, metal-intermetallic laminated (MIL) composites have drawn great interest due to their potential in performing various functions such as heat exchange, thermal management, vibration damping, blast mitigation, ballistic protection and so on. [8] Lamination of intermetallic compounds has made it possible to better utilize intermetallics and boost the applications in structural and aerospace industries. As commonly acknowledged, intermetallic compounds are consisted of solid phases formed with two or more metallic elements, which have different crystal structures from that of the constituents. With appealing features like high melting point, creep resistance, corrosion resistance, high strength, low density, etc., intermetallic compounds have great potentials once properly designed and applied as functional material. These compounds which have ordered crystalline structures and well-definable stoichiometry that distinguish them from other common alloys, are a kind of material that has exceeding strength yet usually are very brittle at room temperature. The brittleness exhibited at room temperature largely limits its development and application for structural uses. In the effort of circumventing such

drawback and making use of other excellent properties, fabrication of intermetallic materials into laminated metal composites is presented as a practical and efficient approach. Other methods like deposition may also be used for fabricating similar composites, yet the cost-effectiveness and scalability are often limited. Since it is usually produced in open air which has minimum requirement on the processing environment, fabrication of MIL involves simple processing and a variety of metal selection. MIL composites are fabricated with alternating layers of component metal foils which undergo heat processing designed to react and form certain intermetallic phases, leaving a final product of alternating layers of residual component metals and newly formed intermetallic compounds. The control of thickness for metal and intermetallic layers in a MIL composite can be finely tuned by adjusting the thicknesses of constituent metal foils and setting of heat treatment, etc.

Comprehensive work has been done on the synthesis of metal-intermetallic lamination in air by Vecchio and others. The standard composite synthesis apparatus setting which requires special equipment and standard procedures have been developed. The successful synthesis of Ti6Al4V-Al_3Ti showed great potentials and advantage in aerospace applications. And a specific stiffness of Ti–Al_3Ti can be as high as twice of steel[5] Based on the method of reactive foil sintering for MIL composite fabrication, the combination of explosion welding and subsequent annealing also presents as a relatively cost-effective technique. The authors suggest that to accelerate the process of complete aluminum dissolution, factors like reaction temperatures above the melting point of aluminum may be considered. Previous work based on Ni-Al binary has been done by Konieczny, in which laminated Ni-(Ni_2Al3 + $NiAl_3$) and Ni-(Ni_3Al + NiAl) composites have been produced in vacuum under heating temperatures 620℃ and 1150℃ respectively. [9] The investigation also shows that the intermetallic phases Ni_2Al_3 + $NiAl_3$ formed at 620℃ may convert to Ni_3Al + NiAl when the composite undergoes another annealing process heated at 1150℃ for 4 h. As for mechanical properties, Ni-(Ni_3Al + NiAl) composites may have a yield strength of 265 MPa, and a tensile strength as high as 875 MPa, and an elongation of 24%. The fracture behavior showed a combination of brittle fracture of Ni_2Al_3 + $NiAl_3$ intermetallic phases and ductile of

residual Ni layers. It also revealed that the presence of continuous Al_2O_3 inclusions may cause delamination in the middle of the composite.

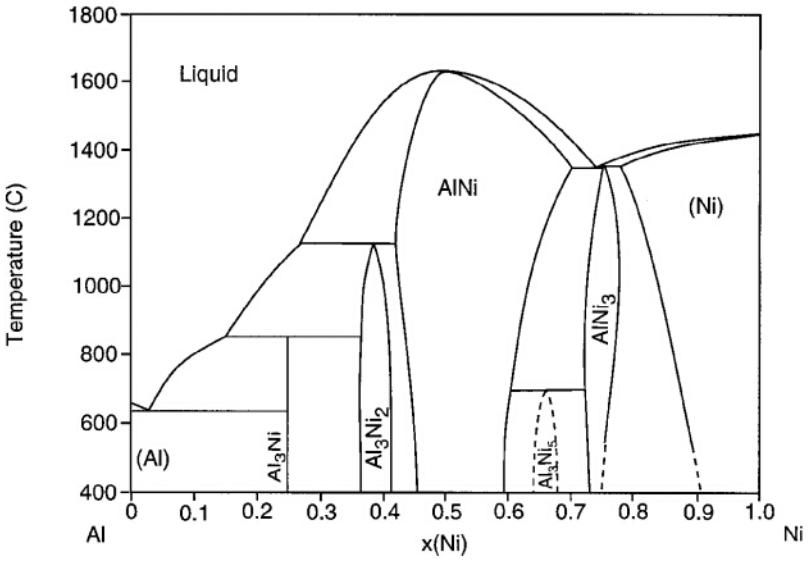

Figure 1.1 Ni-Al binary phase diagram [10]

In the present study, the reactions between nickel and aluminum, nickel alloys including Inconel, and Invar have been studied. Nickel and its alloys are applied widely in various fields, such as aircraft gas turbines, chemical and petrochemical industries, mainly for their excellent resistance against heat and corrosion. Apart from that, commercially pure nickel also has high electrical conductivity and good magnetostrictive properties. Its excellent thermal conductivity also means that it can be used on heat exchangers. [10, 11]

As a family of nickel-chromium-based superalloys with excellent resistance against oxidation and corrosion, Inconel alloys are well suited for applications under extreme circumstances, such as in gas turbine blades and combustors which work under high pressure and high temperature, steam generators in nuclear reactors, automobile turbo systems and exhaust systems and so on. With its excellent resistance to pitting and crevice corrosion, it is widely used in the area of sea water applications. As a more cost-effective substitute of nickel-chromium alloys, nickel-chromium-iron alloys, typically

60% Ni, 20% Cr, and 20% Fe, are also widely used in the form of wire or tape in electrical heating devices.

Invar was first discovered by Charles Édouard Guillaume in 1896, who was rewarded by the Nobel Prize in Physics for this discovery later in 1920. With an approximate composition of 64% iron and 36% nickel, it is also noted as 64FeNi. Well-known for its low coefficient of thermal expansion (CTE), Invar is a single-phase nickel-iron alloy which is often used in precision instruments, antimagnetic watches, seismic creep gauges, valves in motors, cavity resonators, and scientific instruments where dimensional stability is highly required. [12]

In the following chapters, the experimental methods and results were provided for the comparative study among the three types of reactions between aluminum and nickel, aluminum and Invar, as well as aluminum and Inconel respectively.

CHAPTER 2: EXPERIMENTAL METHOD

2.1 Preparatory Work

Three types of nickel foils were used in the experiment, including commercially pure nickel (99.96 at% Ni, 0.04 at% other element), and two types of nickel alloys, Inconel (47.29 at% Ni, 25.40 at% Cr, 20.03 at% Fe, 6.22 at% Mo, 1.06 at% other elements) and Invar (65.63 at% Fe, 32.59 at% Ni, 1.78 at% other elements), to react with commercially pure aluminum (99.84 at% Al, 0.16 at% Fe). All foils were cut into squares with approximate dimensions of 5.08 cm × 5.08 cm (2 inch × 2 inch). To remove the oxide layers and other contaminants, surfaces of the foils were well cleaned by coarse and fine Scotch pads sequentially and rinsed with methanol. Aluminum and nickel foils were stacked in an alternating manner and placed in the composite synthesis apparatus [5]. To provide a better temperature control and reduce heat loss to the environment, ceramic fiber blanket was used to cover the apparatus during the heating process. Multi-nickel samples were made using all three types of nickel foils to study the difference on reactions of pure nickel, Inconel, and Invar with aluminum foils under the same reaction conditions. The stacking sequence is shown in Figure 2.1.

2.2 Heat processing

Pre-heating of the hot press from room temperature (25℃) to the starting temperature (620℃) generally took 2 hours. Heating processes with three different levels of final temperatures were used to study the reaction profiles. The starting temperature of all three processes was 620℃. Both individual and multi Ni-Al samples were made using the heating processes. Individual samples were made of pure Ni,

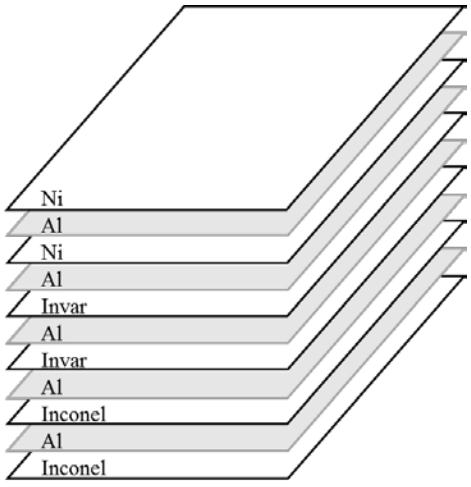

Figure 2.1 Stacking sequence of pure nickel, Invar, Inconel and aluminum foils in an alternating manner.

Invar and Inconel foils individually with Al foils. Sample id and corresponding heating processes are listed in Table 2.1.

Table 2.1 Heating processes for different reaction stages

Heating Process	Starting Temperature/℃	Highest Temperature/℃	Loading/MPa	Sample #
1	620	623	3.45	Pure Ni-Al 1, Multi Ni-Al 1
2	620	636	3.45	Pure Ni-Al 2, Multi Ni-Al 2
3	620	675	3.45, suspended at 650℃, reinstalled at 640℃	Pure Ni-Al 3, Invar-Al 3, Inconel-Al 3 Multi Ni-Al 3

To study the initial stage of reactions, the highest temperature for heating process 1 was 623℃. To study the intermediate stage of reactions, the highest temperature for heating process 2 was 636℃. To study the final stage of reactions, heating process 3 started with 620℃ and heated up to the highest point of 675℃, with the heating rate of 2℃ per hour. Then the temperature was decreased at the rate of 15℃ per hour to 500℃. In all three heating processes, after the temperature dropped to 500℃, it was then left to cool down to room temperature in open air. During heating processes 1 and 2, the samples were loaded onto the hot press under the constant loading pressure of 3.45 MPa (8896 N over 25.8 cm^2).

For heating process 3, the same loading of 3.45 MPa was added to the samples during the initial heating period, in order to provide a compact surface contact between nickel and aluminum foil. Once the temperature reached 650℃ (near to the melting point of aluminum), the loading plate was suspended to avoid aluminum squeezing out. To minimize the impact of internal stresses caused by differences of thermal expansion coefficients between nickel layers and intermetallic layers, 3.45 MPa loading pressure was reinstalled was reinstalled during the cooling process when the dropping temperature reached 640℃. To compare the growth rates, multi-Ni-Al samples were made under

constant temperature at 635℃ for 3h and 9h. Lengths of the intermetallic layers were measured.

2.3 Microstructure and Characterization

All of the samples taken out during different stages of reaction were processed and prepared using conventional metallographic techniques. Samples were mount in Struers LaboPress-3 with 20 kN, heating time of 4 minutes and cooling time of 6 minutes. Mounted samples were later grinded and polished with Stuers Rotopol-2. Grinding process used deposable grind papers with grinding grade of 180 grit, 320 grit, 500 grit, 1200 grit, 2400 grit, and 4000 grit, all under inserted force of 20 N. For the first three grinding grades, grinding time was 3 minutes and 6 minutes for the last three grades. Polishing process was performed on Rotopol-2 with Multidoser. The first two steps of using 6 micron meter DiaDuo diamond suspencion and 1 micron meter diamond suspension both took 6 minutes. For partially reacted samples, to better polish the un-reacted aluminum layers, AP-A Suspension of 5 micron meter and 1 micron meter aluminum polishing suspension were used. Each took 10 minutes with manual dosing for every 2 miuntes. For the final polishing step using Struers OP-U doing, it took 10 minutes and was followed by a final water-rinsing step for 10 minutes to clean out the residual OP-U in tubes. All polishing steps were performed under 15 N.

For metallurgical observation, an Olympus GX51 optical microscope was used with analysis software Pax-it.

X-ray diffraction measurements were performed on Rigaku X-ray diffractometer using Cu K_α radiation. Measured range was from 2θ of 20° through 120° with a step size of 0.02° and 1 second hold time.

A FEI Quanta 600 SEM system with a Bruker X-flash 6160 EDS detector was used for SE and BSE based analysis. Working condition was under 20kV, with a working distance around 11mm.

CHAPTER 3: RESULTS AND DISCUSSION

3.1 Reaction between pure nickel and aluminum

Samples using commercially pure nickel and commercially pure aluminum foils were made. For a near-completion sample, the heating process took 21.5 h, starting with temperature of 620℃, and finally reaching the highest point of 675℃. To study the reaction progress, interrupted reaction method is applied. Pure nickel-aluminum samples labeled as Pure Ni-Al 1, Pure Ni-Al 2, and Pure Ni-Al 3 were made, which were respectively heated for 2.5 h reaching at temperature of 623℃, 9 h reaching at temperature of 636℃, and 21.5 h and 675℃ for near-completion reactions. Multi-nickel samples containing two sheets of pure nickel foils, two sheets of Invar foils and two sheets of Inconel foils, together stacked with aluminum foils in the alternating sequence were made (Figure 2.1). Samples labeled as Multi-Ni-Al 1, Multi-Ni-Al 2, and Multi-Ni-Al 3 were made using heating processes 1, 2, and 3, which was heated up to 623℃, 636℃, and 675℃ respectively. In order to let the intermetallic phases further develop and be more distinct, a piece cut from Multi-Ni-Al 3, labeled as Multi-Ni-Al-Annealed, went through an extra annealing process at 650℃ for 2 h.

As observed from the reacted samples, even with the help of real-time monitoring of the temperature change, a temperature gradient always existed among the layers within the same sample, varying to certain degrees which may lead to the difference in thickness of intermetallic layers, for example, at the initial stage of reaction, nodules were formed on some locations while on other locations thin layers already formed, which suggests that the overall homogeneity within the same sample is hard to control.

The reaction profile between pure nickel and aluminum sheets can be classified into four stages: stage one of solid-solid reaction at temperatures below the melting temperature of Al; stage two of solid-liquid reaction; stage three of further growth of intermetallic layers; and final stage of reaction completion.

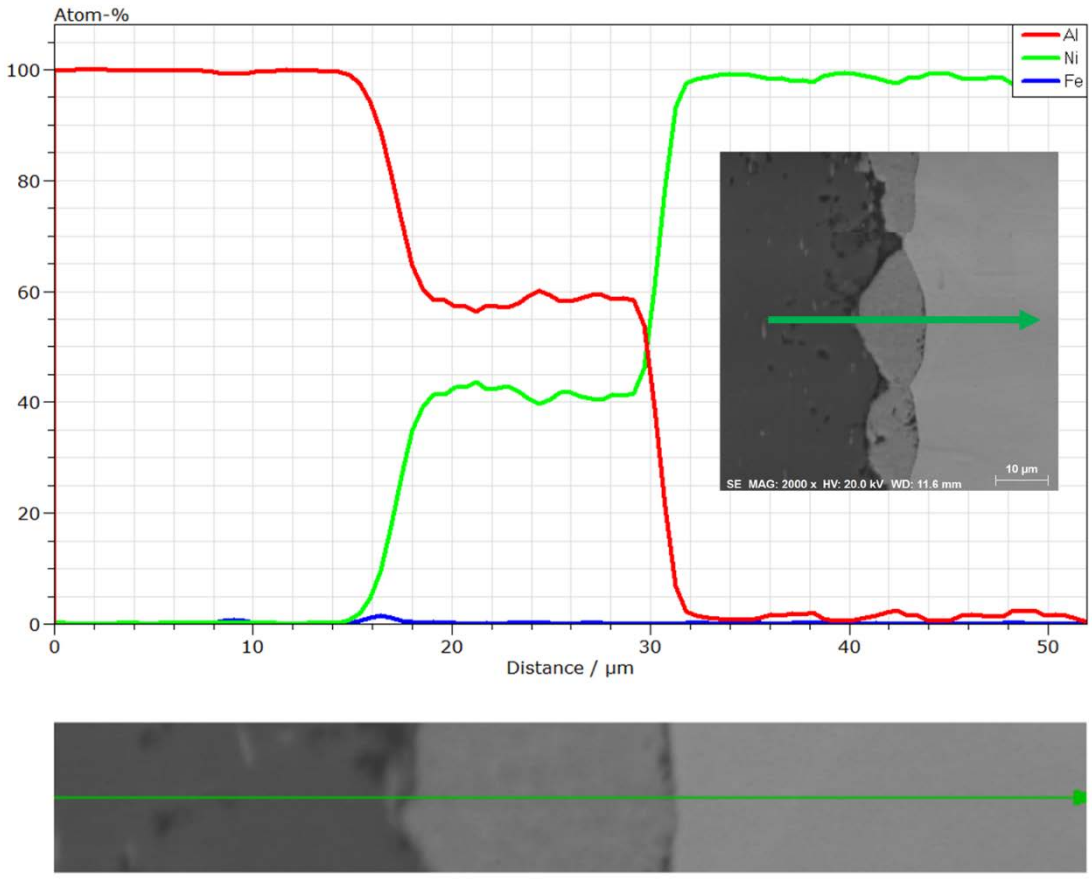

Figure 3.1.1 Linescan across a nodule found in sample Pure Ni-Al 1. MAG: 2000x; HV: 20.0 kV; WD: 11.6mm.

In the case of Ni-Al binary system, at the first stage of reaction when the temperature was within the range of 620℃ - 660℃, the initial intermetallic formed was Al_3Ni_2. In this stage, Al atoms were the only major diffusing species. As shown in Figure 3.1.1, nodules of Al_3Ni_2 were first formed at the interface between Ni and Al layers. In stage 2, as temperature reached the melting point of Al, while nodules of Al_3Ni_2 grew larger and merged into layers, the presence of the second intermetallic phase occurred; a layer of Al_3Ni start to form at the front of Al_3Ni_2 layer, as revealed by the compositional linescan result in Figure 3.1.2. Due to the large difference on melting temperatures between Al (660℃) and Ni (1455℃), it was as expected that among the multiple Ni-Al intermetallic phases, Al-rich phases (Al_3Ni_2, Al_3Ni) were found in the reaction. Once the temperature reached the melting point of Al, the occurrence of solid-liquid reaction

between Ni and liquid Al would further accelerate the formation of both intermetallic phases. In stage 3 of intermetallic layer expansion, both layers of intermetallic phases continued to advance into the center of Al layer. In the final stage where original Al layer was nearly consumed in completion, two major intermetallic phases, Al_3Ni_2 and Al_3Ni occupied where the Al layer originally was. This result coincides with the work done by M. Knonieczny, in which the heat processing was set in vacuum at a temperature of 620℃ and a composite comprising Ni-(Al_3Ni_2 + Al_3Ni) was obtained.

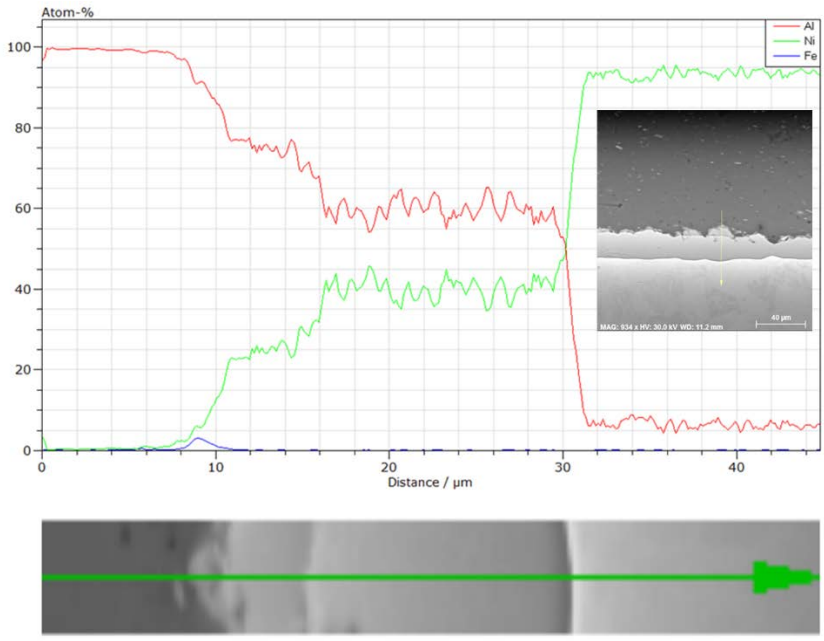

Figure 3.1.2 Linescan across a more reacted region found in sample Pure Ni-Al 1. MAG: 934x; HV: 30.0 kV; WD: 11.2mm.

As shown in Figure 3.1.2, from the compositional linescan across the newly formed intermetallic layers, a Fe-rich minor phase was formed at the front. During the reaction, as limited by the selection of raw materials, when the intermetallic layers were growing towards the center of Al layer, Fe atoms in the Al foil were pushed out and participated in the reaction with Ni and Al, although in a small amount, forming the third type of intermetallic compound at the front of advancing Al_3Ni layers, which was later identified as $Al_{80}Fe_5Ni_{15}$, an intermetallic compound with similar atomic ratio to $Fe_{0.7}Ni_{1.3}Al_9$. Thin layers of $Fe_{0.7}Ni_{1.3}Al_9$ from both advancing sides met and formed a

centerline, which was originally the centerline of Al foil before reaction, occupying the middle of two intermetallic layers. The ratio of widths for the two major phases is approximately Al_3Ni_2: (Al_3Ni+ $Al_{80}Fe_5Ni_{15}$) = 2:1. The linescan result in Figure 3.1.2 also suggested that when the width of Al_3Ni_2 intermetallic layer reached 15 μm, the second intermetallic compound, Al_3Ni, started to form at the front.

Notably, as Figure 3.1.6 illustrates, the presence of a centerline was caused by the formation and accumulation of $Al_{80}Fe_5Ni_{15}$, which was the result of reaction between impurity Fe atoms with Al and Ni.

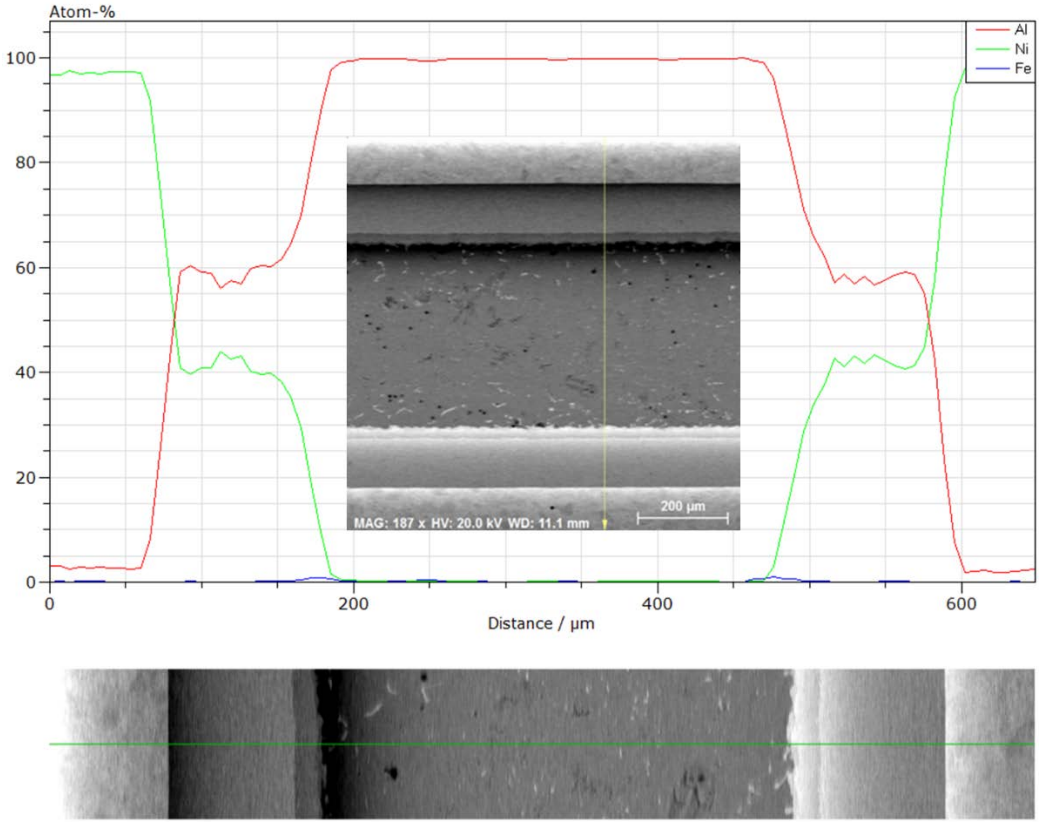

Figure 3.1.3 Linescan of Al_3Ni_2 and Al_3Ni layers in sample Pure Ni-Al 2. MAG: 187x; HV: 20.0 kV; WD: 11.1mm.

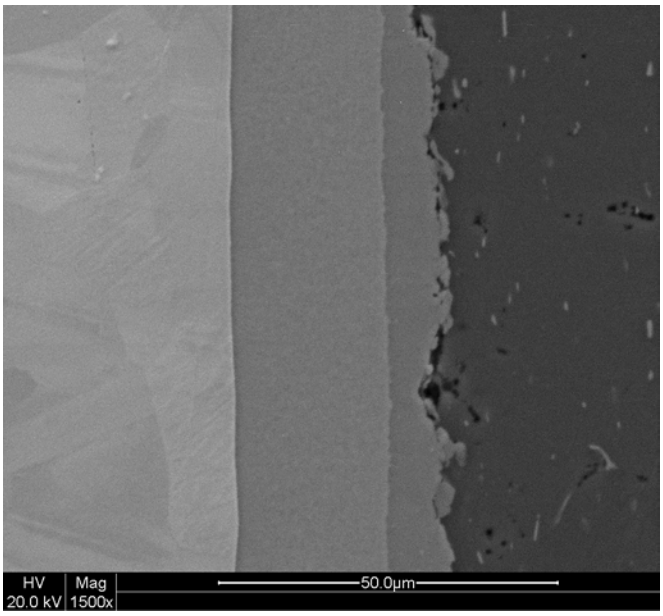

Figure 3.1.4 BSE picture of nickel, Al_3Ni_2, and Al_3Ni layers from sample Multi-Ni 1. The growth of Al_3Ni_2 is relatively dominant in this case.

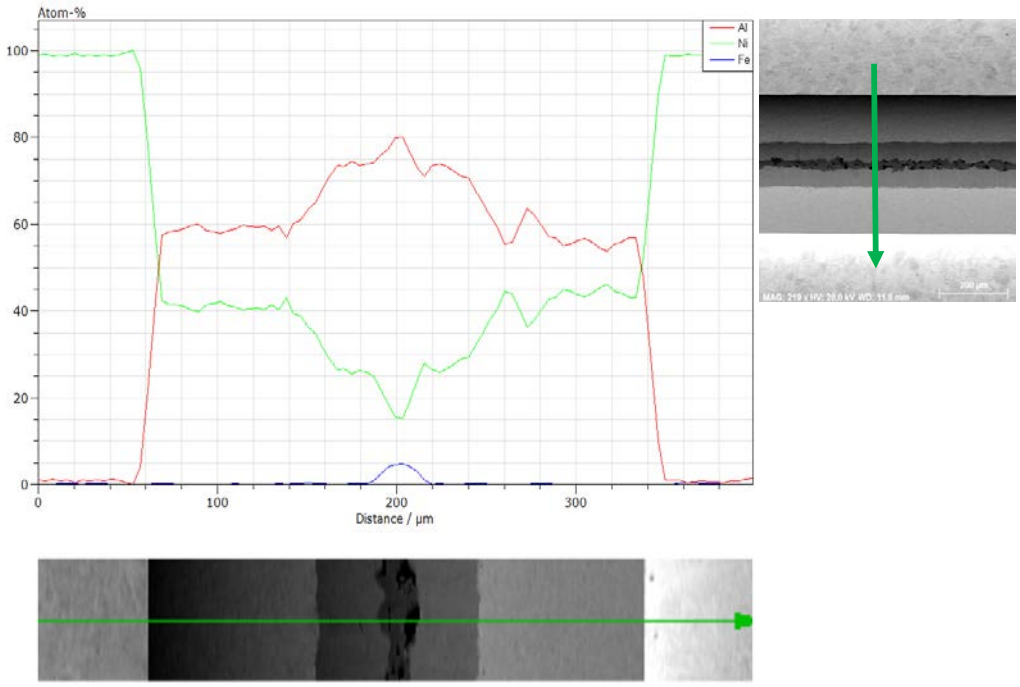

Figure 3.1.5 Linescan across the intermetallic layers found in the near-completion sample Pure Ni-Al 3. MAG: 219x; HV: 20.0 kV; WD: 11.8mm.

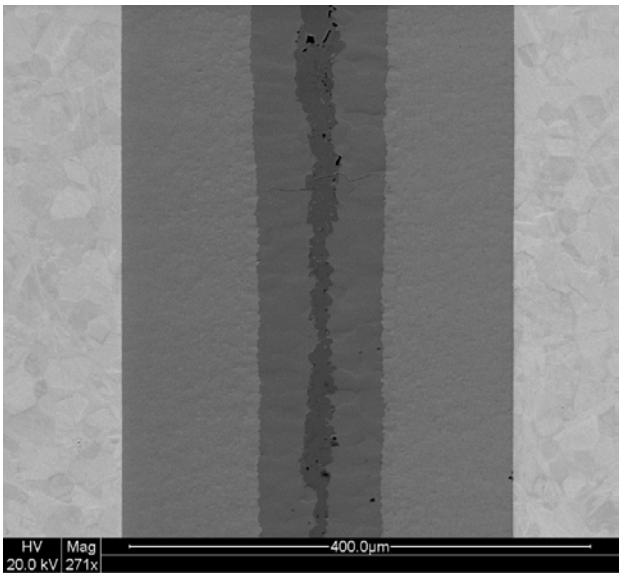

Figure 3.1.6 BSE picture of nickel, Al_3Ni_2, and Al_3Ni layers from sample Multi 2.

As showed in BSE picture of annealed multi-nickel sample (Figure 3.1.7), after heated at 650℃ for 2 hr, the intermetallic layer of Al_3Ni transformed into an annealed layer of Al_3Ni_2 in which the orientation of Al_3Ni was retained, while Figure 3.1.8 shows the difference in orientations of the major Al_3Ni_2 layer and the annealed one. If the annealing process goes for a longer time and/or under a higher temperature, formations of other Ni-rich intermetallic phases such as AlNi and Ni_3Al, can be expected. Figure 3.1.9 compares the heats of formation for Ni-Al intermetallic compounds. Yet, notably, the generation of cavities in the centerline of $Al_{80}Fe_5Ni_{15}$ was caused be the depletion of Al.

To compare the growth rates of different intermetallic phases, multi-Ni-Al samples heated at 635℃ for 3h and 9h were made. As measured from the pure Ni-Al regions, the total intermetallic thickness was 51.3 μm for 3h and 87.7 μm for 9h.

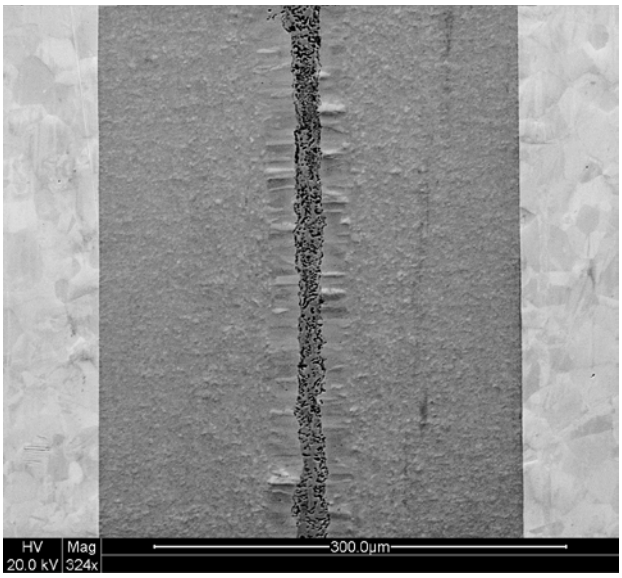

Figure 3.1.7 BSE picture nickel and Al_3Ni_2 layers from sample Multi-Ni-Al-Annealed. During further reaction, the Al_3Ni layer grow into Al_3Ni_2.

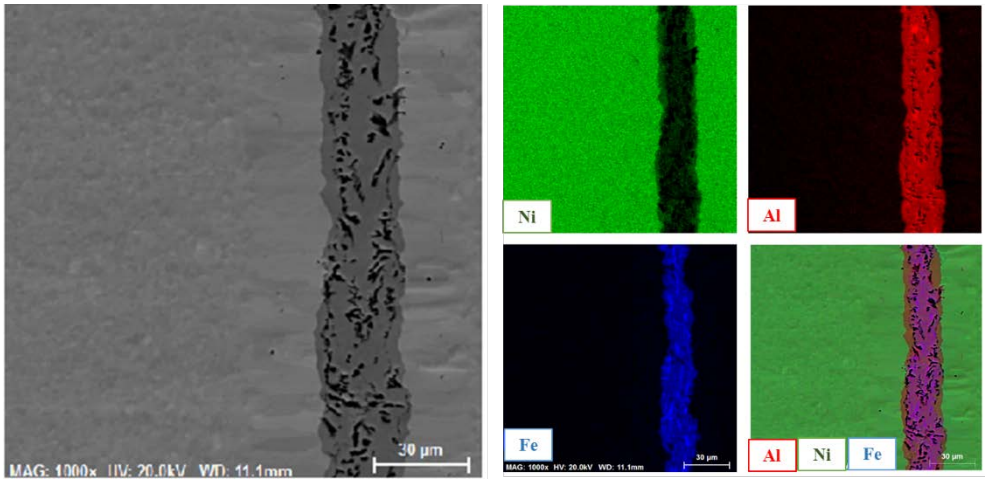

Figure 3.1.8 Mapping over annealed Ni-Al layer. Magnification: 1000x; HV: 20kV; WD: 11.1mm.

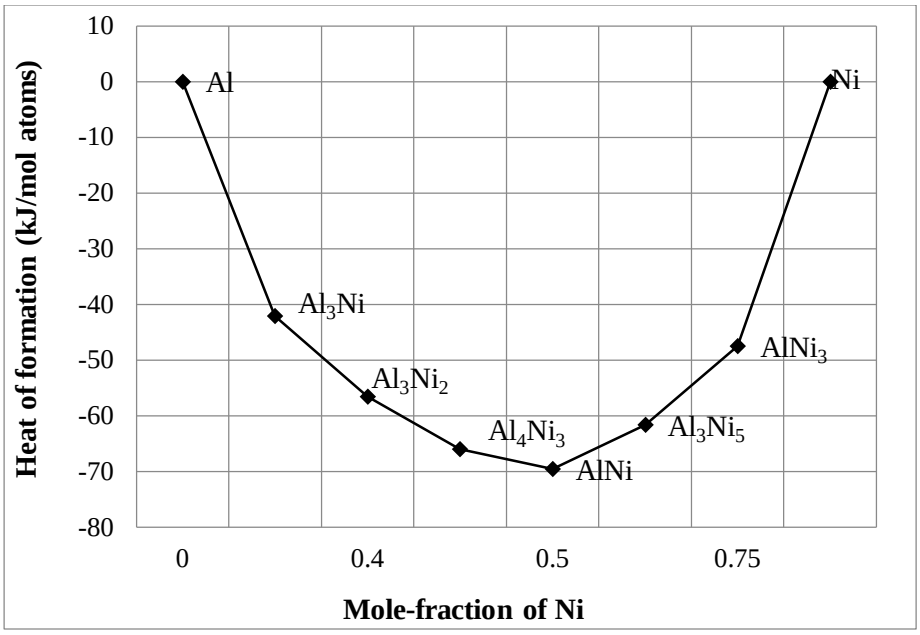

Figure 3.1.9 Heats of formation for Ni-Al intermetallic compounds. [13]

3.1.2 Nano-Indentation Tests of Ni-(Al_3Ni_2+Al_3Ni)

The Nano Indenter® XPW is a computer-controlled indenter from MTS System. It is used to test the young's modulus and hardness of the specimen. From the tests run on unreacted pure nickel foils, a Young's modulus with an average value of 172.9 GPa is obtained, in comparison with a reference value of 200 GPa. Hence a variation of 13.55% between the measured value and the actual value is expected.

For each set of indentation tests, in every morphologically distinctive layer, five indentation locations were picked in parallel to each other. To obtain credible test results, a distance of 80 μm was set between each layer of interest. As can be seen from Figure 1 and 2, the moduli and hardness values show an increasing tendency over the intermetallic regions, compared to the residual pure nickel regions after heat treatment. As shown in the chart, in a near-completion pure nickel-aluminum MIL composite sample, the Young's modulus in formed intermetallic layers of Al_3Ni_2 has an average value of 157.8 GPa and hardness of 4.2 GPa, while the modulus of Al_3Ni has an average value of 188.9 GPa and hardness of 9.7 GPa. Both modulus and hardness have been significantly

improved over the intermetallic areas in the composite comparing to the constituent element of nickel.

Table 3.1 Modulus and hardness results on Ni-(Al_3Ni_2+Al_3Ni) sample

	Modulus/GPa	Hardness/GPa
Residual Ni layer	126.9	1.2
Al_3Ni_2	157.8	4.2
Al_3Ni	188.9	9.7

Graph 3.1.1 shows the transition of modulus at max load from one residual nickel layer towards the central of intermetallic layers, and to the other residual nickel layer again in the near-completion sample using commercially pure nickel and aluminum foils. The transition of modulus from the pure nickel side across the Al3Ni2 and Al3Ni intermetallic layers showed an ascending tendency, while suddenly dropped in the centerline. Graph 3.1.2 shows the transition of hardness at maximum load from one residual nickel layer towards the center of intermetallic layers, and to the other residual nickel layer again in the near-completion sample using commercially pure nickel and aluminum. As can be seen from the graph, the average hardness values in both intermetallic layers were significantly higher than the residual pure nickel layer.

Graph 3.1.1 The transition of modulus at maximum load in pure Ni-Al sample.

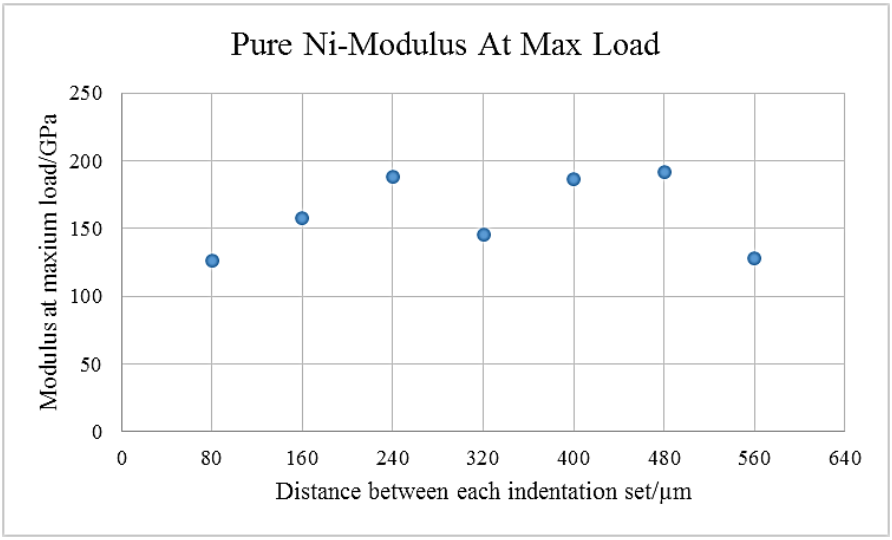

Graph 3.1.2 The transition of hardness at maximum load in pure Ni-Al sample

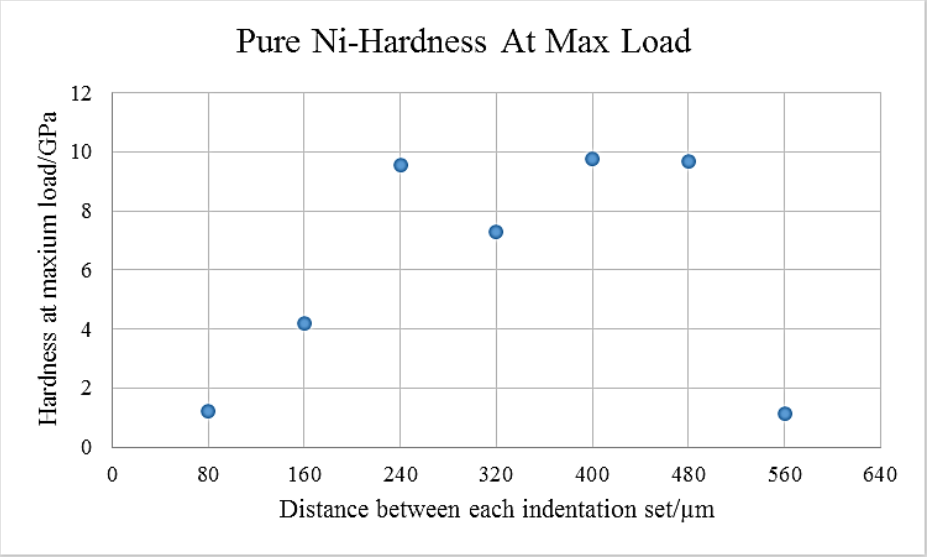

3.2 Reaction between Invar and Aluminum

Samples using Invar (Fe64Ni) foils and commercially pure aluminum foils were made. The interrupted reaction method was then used in tests stopping at different temperatures. For the near-completion sample, the heating process was the same as Pure Ni-Al 3, which took 21.5 h with a starting temperature of 620℃ that gradually reached up to 675℃. As was observed in Pure Ni-Al samples, the growth rates of intermetallic layers were different, which led to a varying thickness of the reacted layers. This was probably caused by the temperature gradient existed among the layers.

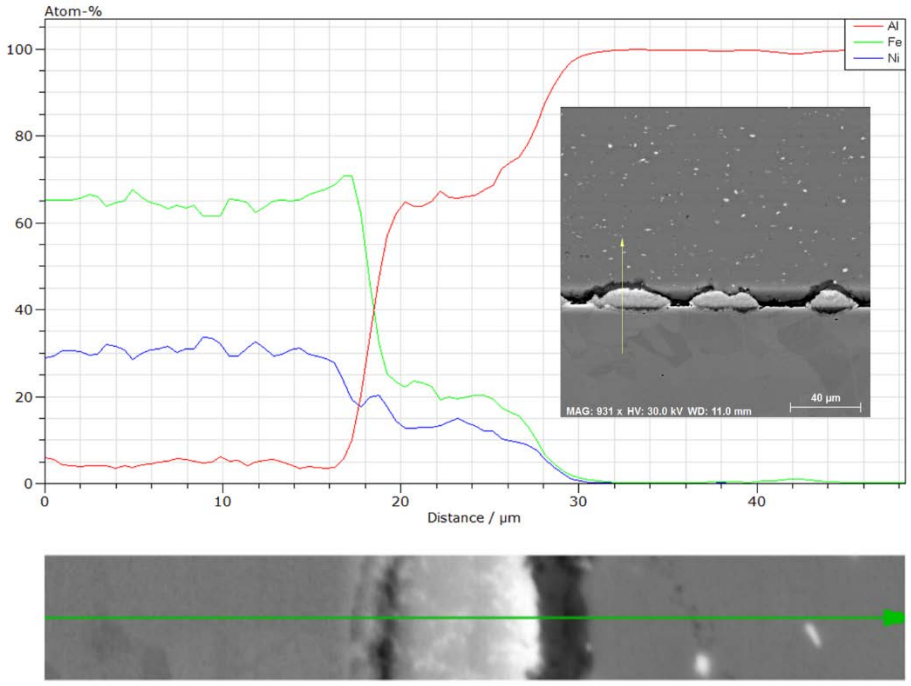

Figure 3.2.1 Linescan across a newly formed nodule between Invar and Al layers from sample Multi-Ni. MAG: 931x; HV: 30.0 kV; WD: 11.0mm.

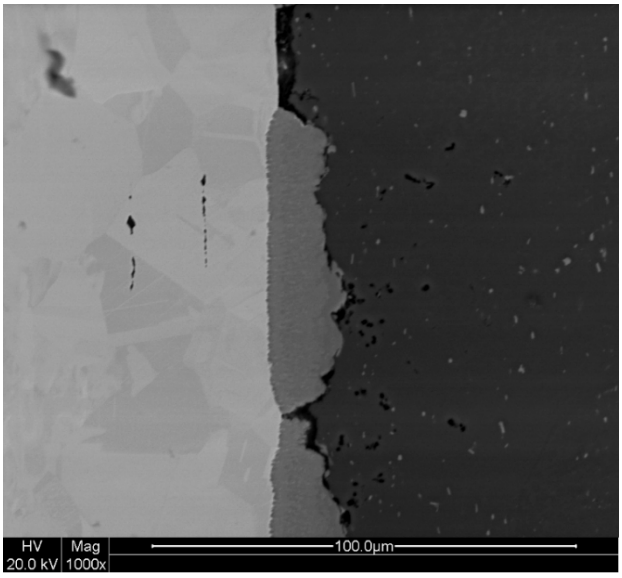

Figure 3.2.2 BSE picture of Invar layer from sample Multi-Ni 1 showing two-phase nodules grow into layers.

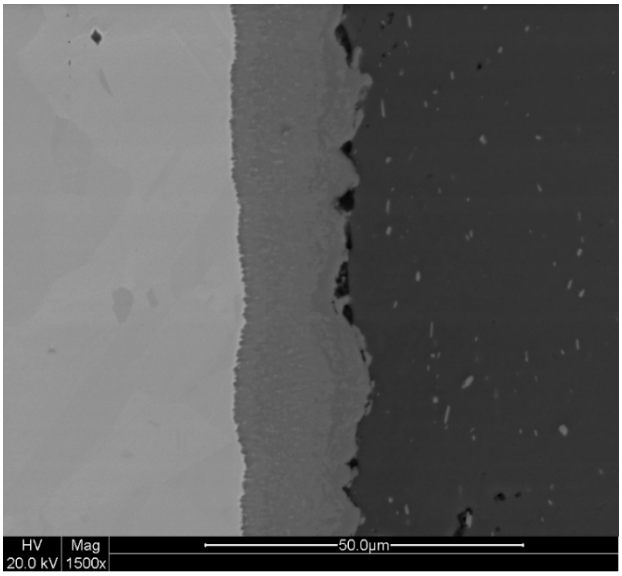

Figure 3.2.3 BSE picture of Invar layer on another location from sample Multi-Ni 1 showing further growth of two-phase layers.

As shown in Figure 3.2.1 and Figure 3.2.2, at the very beginning of the reaction between Invar and aluminum foils, nodules of $Al_{75}Fe_{20}Ni_{15}$ first formed at the interface. As the reaction continued, a thin layer of $Al_{80}Fe_{15}Ni_5$ formed adjacent to the Invar side as shown in Figure 3.2.3. Yet from a mapping of element compositions which was taken at a selected area over the same intermetallic regions, shown in Figure 3.2.4 as Al was represented by the color red, Ni by green, and Fe by blue, it suggested that the distribution of elements were not uniform; at the front of the advancing intermetallic layer, it had a slightly richer Ni content, which may be contributed by the difference in diffusion coefficients of Ni and Fe in Al. The mapping results of Invar regions from sample Multi-Ni 3 is shown in Figure 3.2.11. Two Ni-rich stripes were formed in the center of the intermetallic.

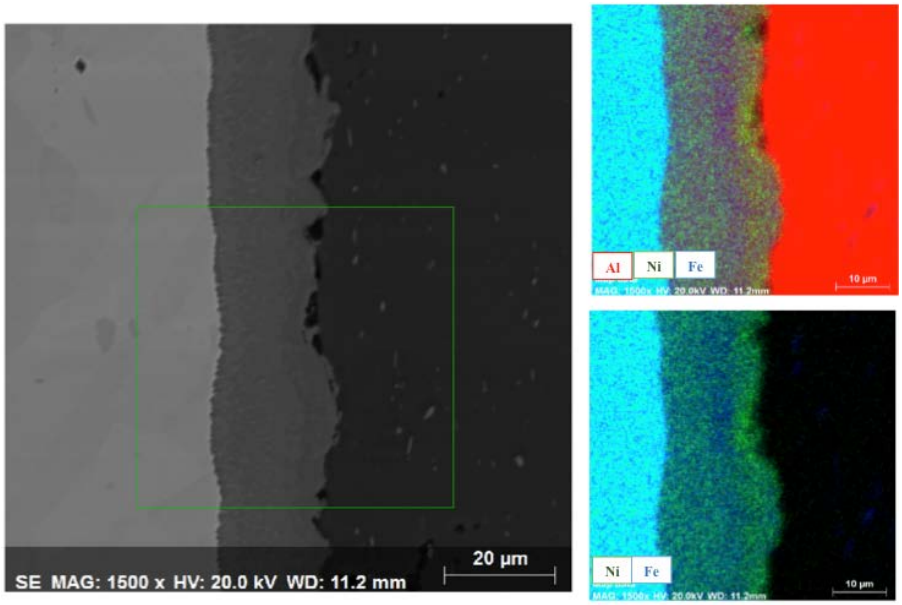

Figure 3.2.4 BSE mapping results of Invar layer over the same location in Figure 3.2.3, from sample Multi-Ni-Al 1 showing the distribution of Ni (green), Fe (blue), and Al(red). MAG: 1500x; HV: 20.0 kV; WD: 11.2mm.

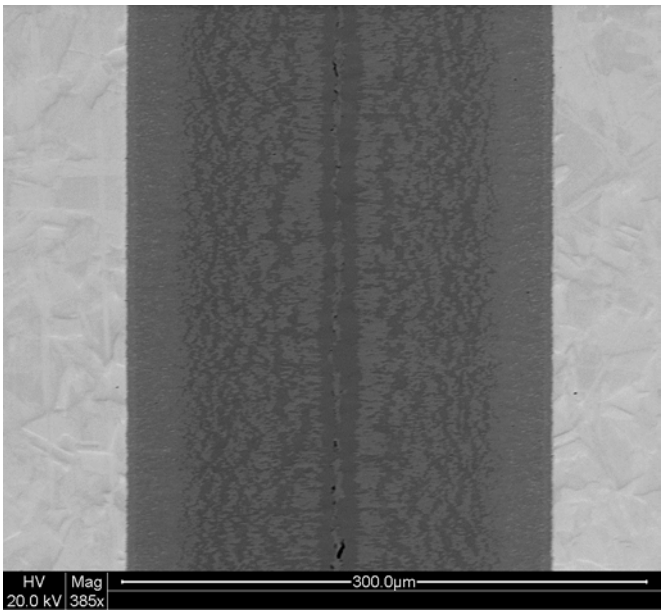

Figure 3.2.5 BSE picture of Invar regions from sample Multi-Ni-Al 2.

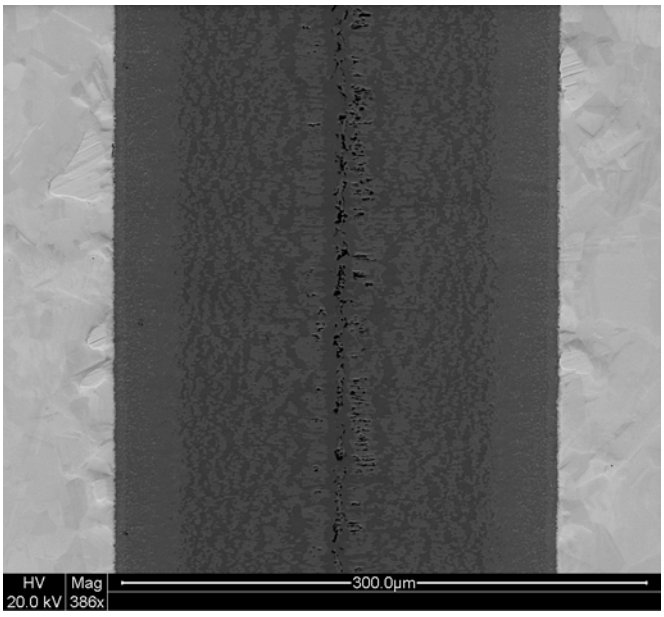

Figure 3.2.6 BSE picture of Invar regions from sample Multi-Ni-Al-Annealed.

Figure 3.2.5 and Figure 3.2.6 illustrate the changes on microstructures before and after the annealing process. Before annealing, the compositions in each intermetallic phase varied slightly from the Invar side to the middle of the intermetallic layer. After annealing, no obvious changes were observed under the optical microscope, except that similar to what was observed in the annealed pure Ni-Al portions, cavities were formed in the center due to the depletion of Al. The widths of Ni-rich layers in the center were decreased, consumed by the formation of more Fe-rich phase. In the annealed sample, the Invar regions showed an overall consistent phase distribution, with stabilized compositions in each phase. In the final stage, two phases formed were $Al_{84}Fe_9Ni_7$, presented as the darker areas, and $Al_{79}Fe_{16}Ni_6$, presented as the brighter areas in Figure 3.2.6.

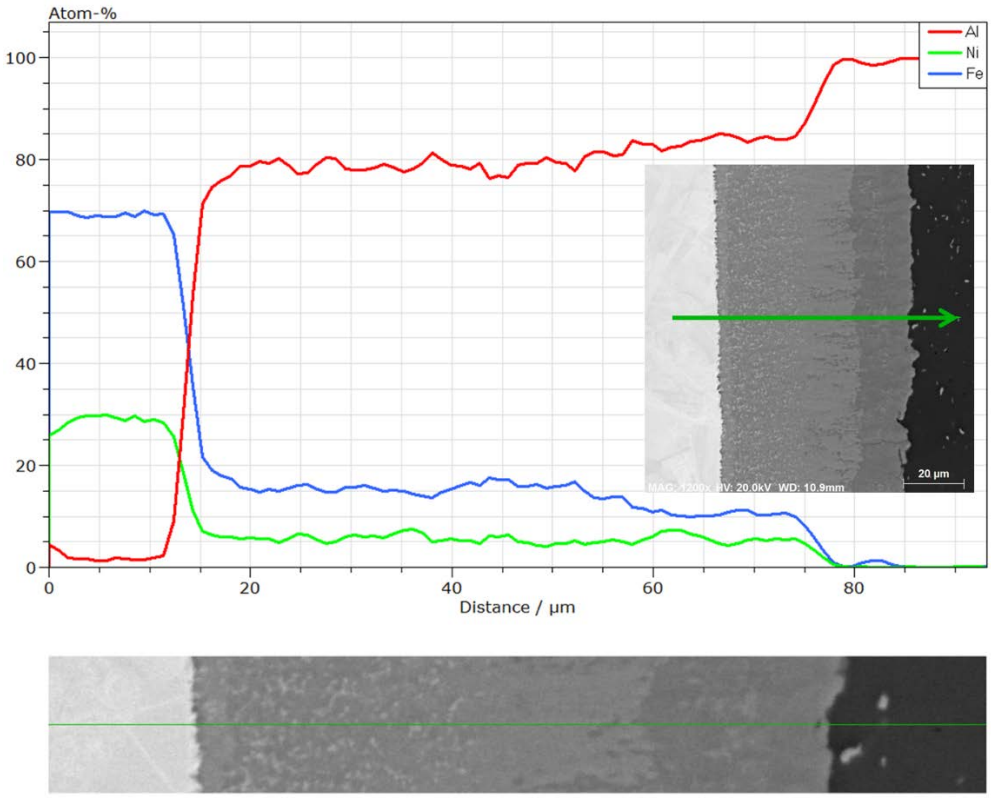

Figure 3.2.7 Linescan across intermetallic layers between Invar and Al layers in Multi-Ni-Al 2 sample.

Figure 3.2.7 shows the linescan result across the overall intermetallic layers in Invar regions from Multi-Ni-Al 2. Figure 3.2.8-10 are the regional (BSE) images across the intermetallic regions from the Invar end to the Al end at higher magnifications. From Figure 3.2.8, the thin layer adjacent to the Invar layer has a chemical composition of $Al_{72}Fe_{19}Ni_9$, and Ni-rich particles with composition of $Al_{76}Fe_{16}Ni_8$ were formed near to the side of unreacted Invar layer. In Figure 3.2.9, the intermetallic phase in the middle region is $Al_{78}Fe_{16}Ni_6$. The intermetallic phase in the region adjacent to the unreacted Al side is $Al_{83}Fe_{10}Ni_7$.

In the isothermal multi-Ni-Al samples heated at 635℃ as measured from the Invar-Al regions, the total intermetallic thickness was 35.7 μm for 3h and 58.7 μm for 9h.

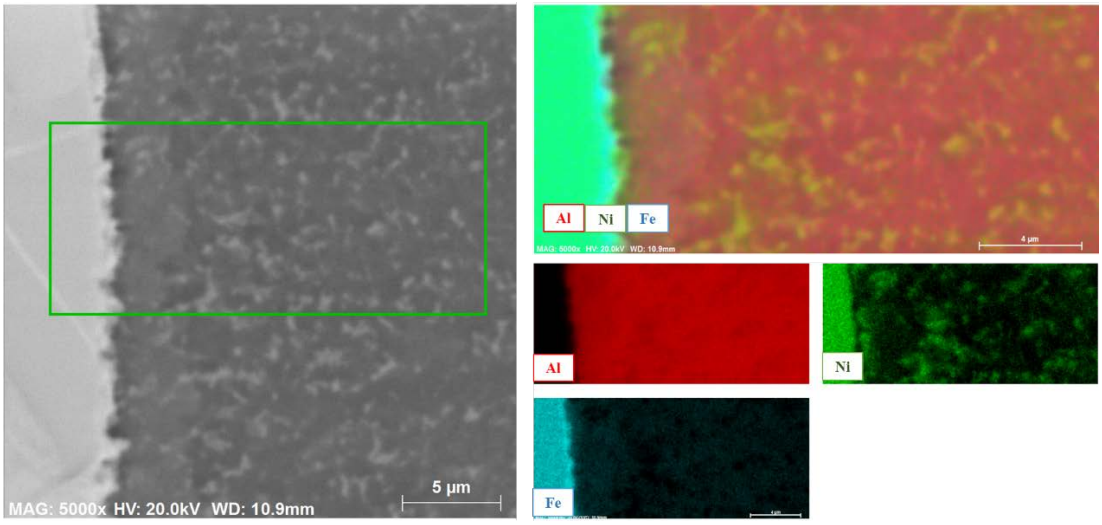

Figure 3.2.8 BSE mapping on the localized region 1 adjacent to Invar layer in Multi-Ni-Al 2. MAG: 5000x; HV: 20kV; WD: 10.9mm.

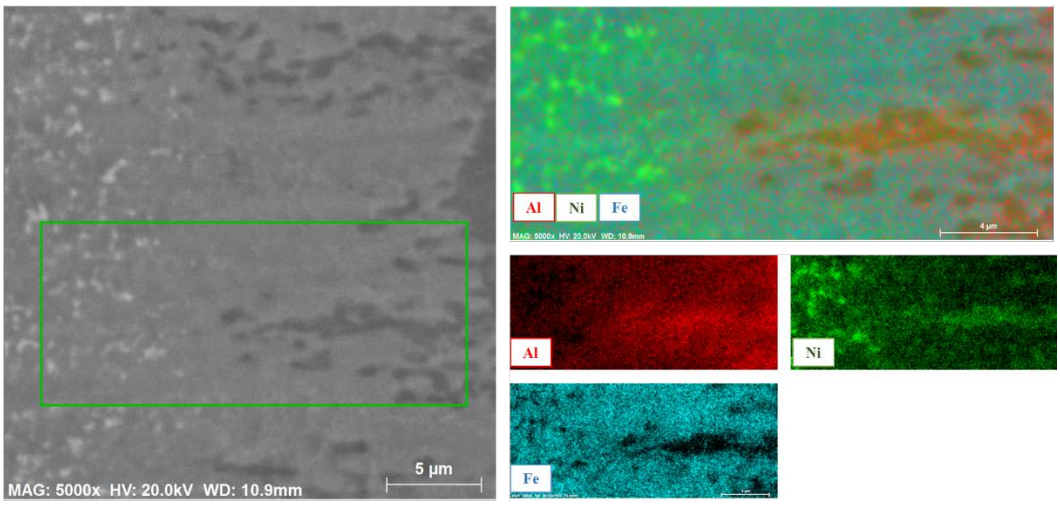

Figure 3.2.9 BSE mapping on the transitional region 2 in Multi-Ni-Al 2. MAG: 5000x; HV: 20kV; WD: 10.9mm.

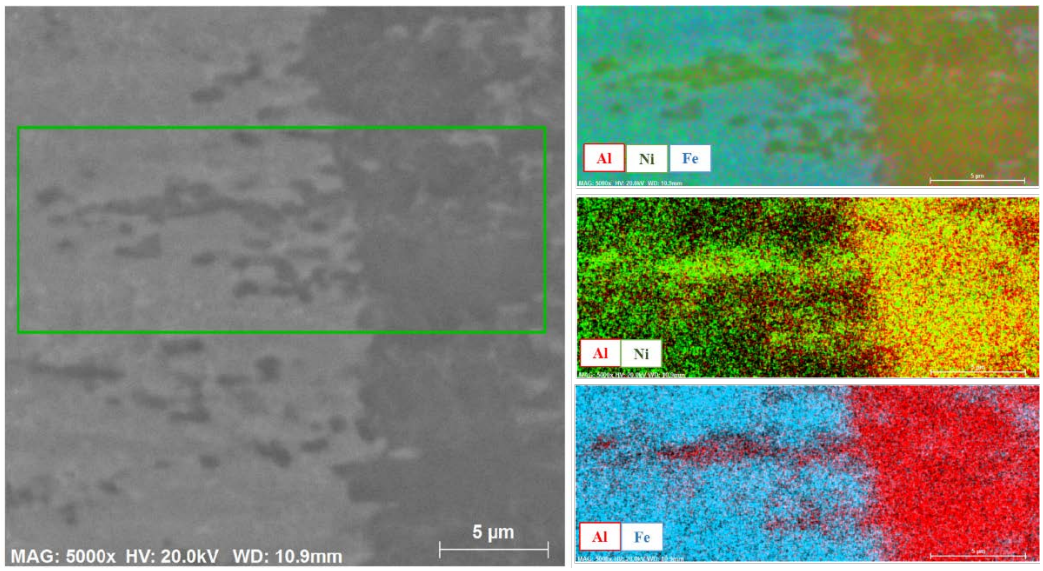

Figure 3.2.10 BSE mapping on the localized region 3 at the front end in Multi-Ni-Al 2. MAG: 5000x; HV: 20kV; WD: 10.9mm.

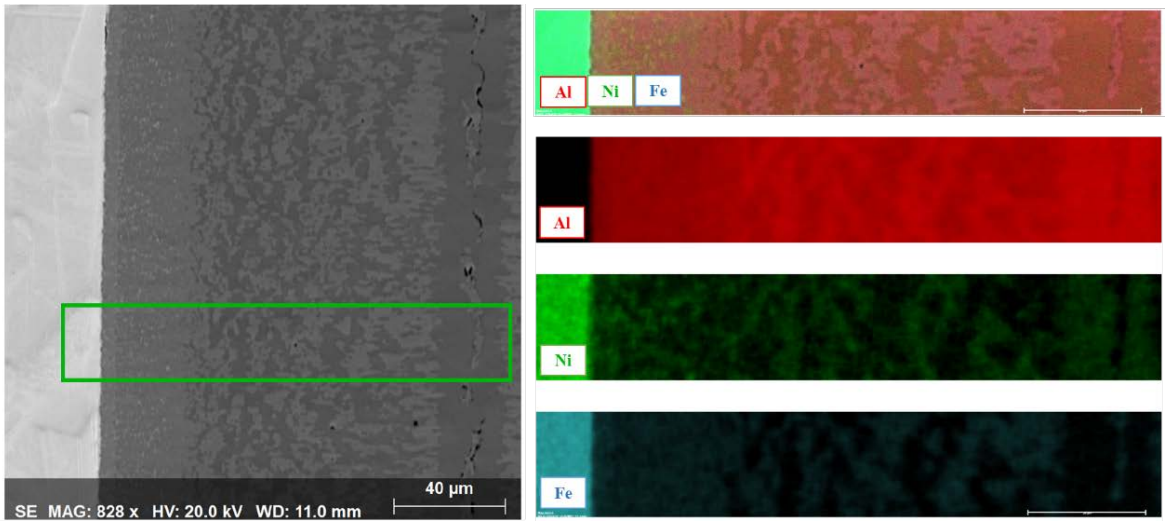

Figure 3.2.11 BSE mapping results of Invar layers from sample Multi-Ni-Al 3.

3.2.2 Nano-Indentation Tests for Invar-Al

The testing method was the same as the pure nickel sample tests. For each set of indentation tests, in every morphologically distinctive layer, a matrix of 5 x 7 indentation locations were selected with a point-to-point distance of 80 µm. Among the 7 tested sets, 4 sets were located in the invar layer due to the limit in indents location selection. As can be seen from Table 3.2, the moduli show a slightly increase yet still relative stable tendency over the intermetallic regions and the residual Invar regions after heat treatment. Yet the hardness shows a significant increase comparing the reacted regions with unreacted Invar layers. Graph 3.2.1 shows the transition of modulus at max load from one residual Invar layer towards the center of intermetallic layers, and to the other residual nickel layer again. The values of modulus of Invar and reacted intermetallics are close, with a difference of around 40 GPa.

Table 3.2 Modulus and hardness results obtained on Invar and intermetallics

Indent Location	Modulus/GPa	Hardness/GPa
Invar	117.8	1.5
Two-phase intermetallic layer	154.0	7.5
Center ($Al_{84}Fe_9Ni_7$)	120.3	4.6

Graph 3.2.1 The transition of modulus at maximum load in Invar-Al layers.

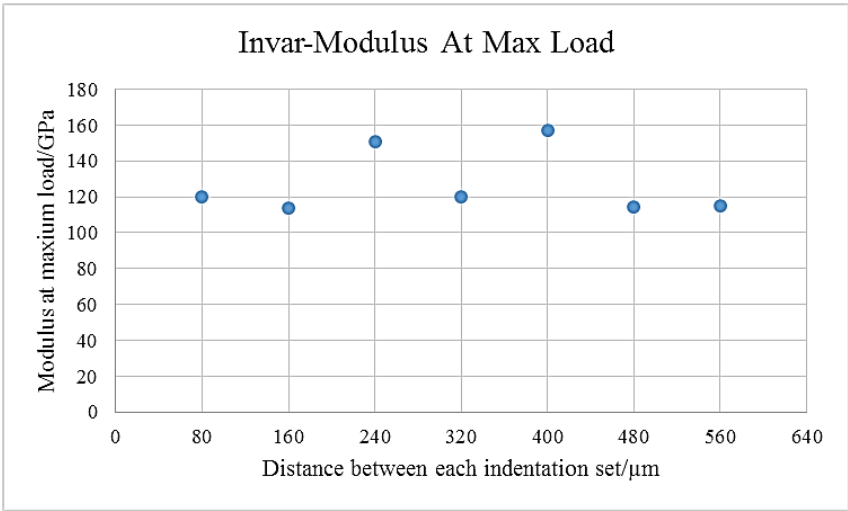

Graph 3.2.2 The transition of hardness at maximum load in Invar-Al layers.

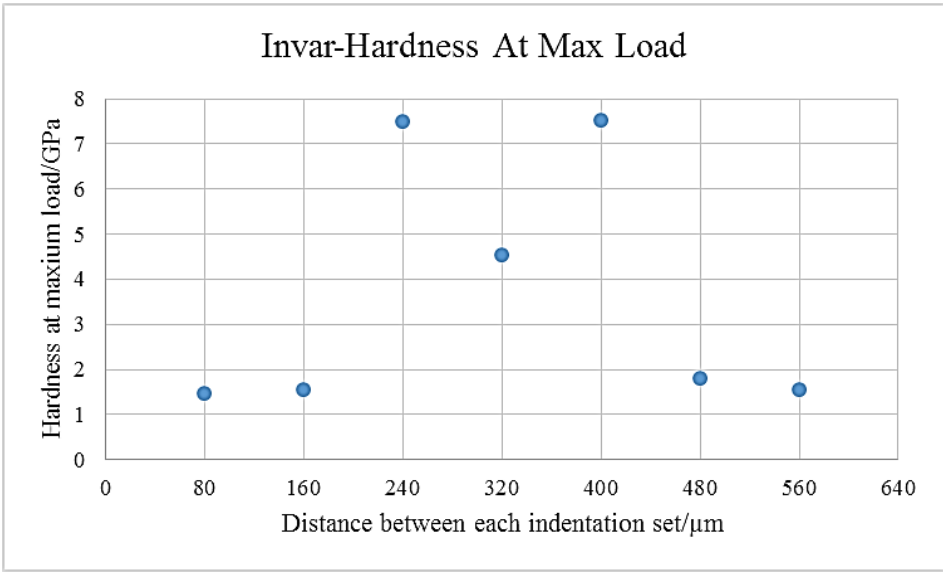

3.3 Reaction between Inconel 625 and Aluminum

In the family of Nickel-Chromium-based superalloys with excellent resistance against oxidation and corrosion, Inconel alloys are widely used for applications under extreme circumstances, such as high pressure and high temperatures. In the isothermal multi-Ni-Al samples heated at 635℃, measured from the Inconel-Al regions, the total intermetallic thickness was 65.7 μm for 3h and 89.7 μm for 9h.

As shown in Figure 3.3.1 and Figure 3.3.2, at the very beginning of the reaction between Inconel and aluminum foils, the small nodule of $Al_{83}Cr_5Fe_4Ni_7Mo$ first formed at the interface between Inconel and aluminum layers. In the larger nodule, two intermetallic compounds, $Al_{84}Cr_3Fe_3Ni_9Mo$ (Ni~9.0at %) and $Al_{80}Cr_6Fe_5Ni_7Mo$ (Ni~7.1at %) were formed. From the mapping result over Inconel nodules from Multi-Ni-Al 1 in Figure 3.3.2, there was an obvious thin layer of $Al_{85}CrFeNi_{13}Mo$ with higher Ni content (Ni~12.9at %) formed at the advancing front of the newly formed nodule. Other elements, Fe, Cr, and Mo were relatively uniformly distributed within the nodule. The reaction continued and the nodules grew into intermetallic layers as shown in Figure 3.3.3.

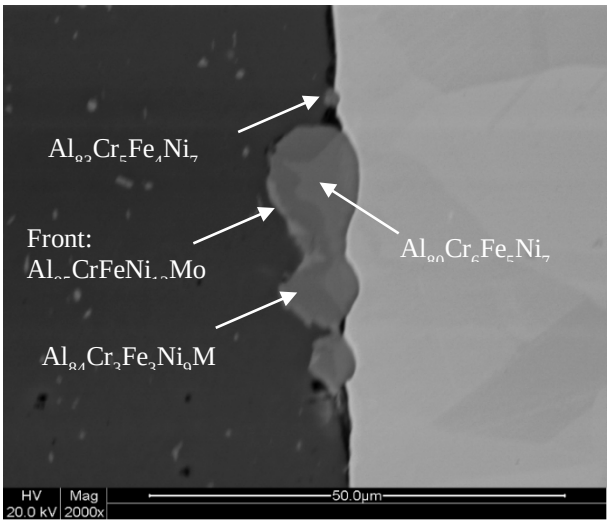

Figure 3.3.1 BSE picture of Inconel nodules from sample Multi-Ni-Al 1 showing the beginning of the reaction when phases started to form.

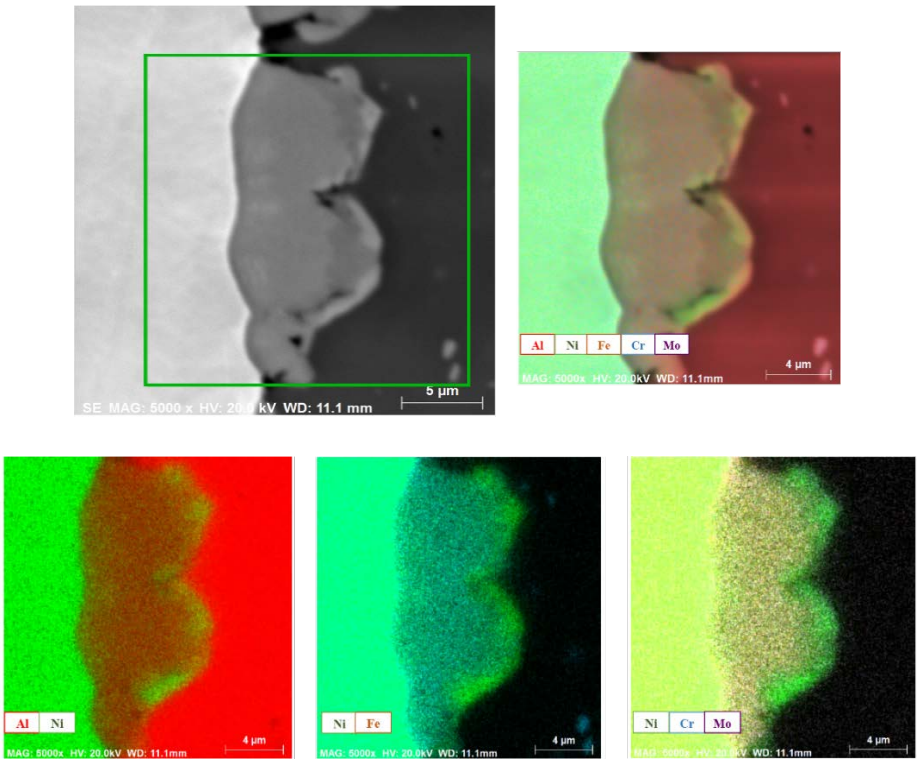

Figure 3.3.2 Mapping of Inconel nodules from sample Multi-Ni-Al 1. MAG: 5000x; HV: 20kV; WD: 11.1mm.

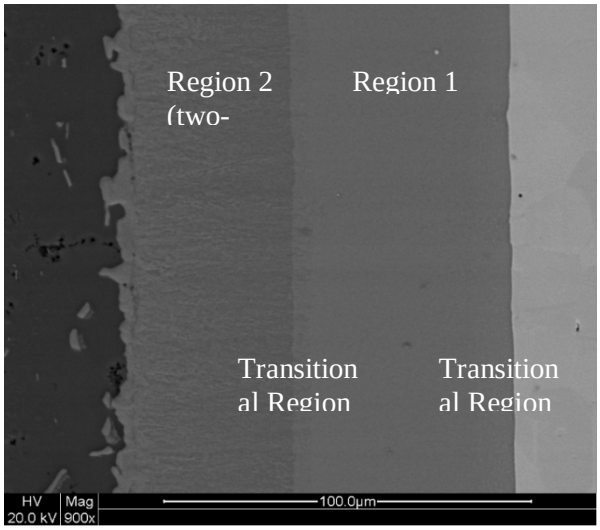

Figure 3.3.3 BSE picture of two major regions formed in Inconel layers in the Multi-Ni-Al 2 sample.

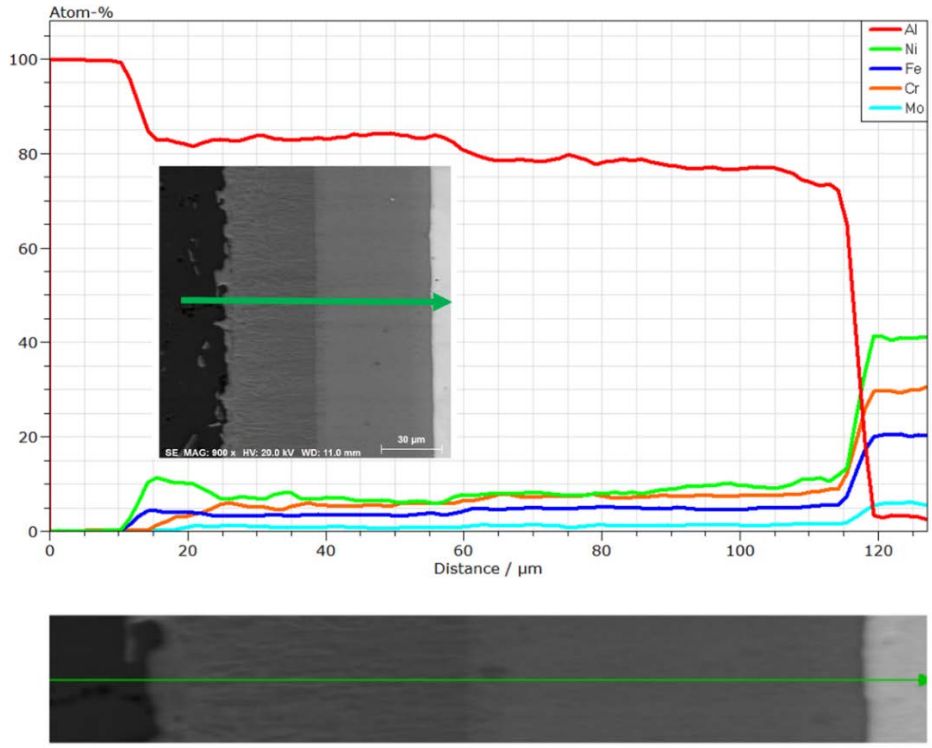

Figure 3.3.4 Linescan across intermetallic layers in Inconel regions from sample Multi-Ni-Al 2. MAG: 900x; HV: 20.0 kV; WD: 11.0mm.

Figure 3.3.3-5 illustrate the chemical compositions over the intermetallic layers. As noted in Figure 3.3.3, apart from the advancing front towards the Al side with particularly high Ni content, two major intermetallic regions and two transitional zones were formed. From the linescan result over intermetallic layers in Inconel regions from sample Multi-Ni-Al 2 (Figure 3.3.4), the presence of two major intermetallic regions 1 and 2 was featured with the change in Al contents. Region 1, which was adjacent to the Inconel layer, had a slightly lower Al content below 80at%, at approximately 76at %, while region 2 had higher Al content at around 83at %. Figure 3.3.5 shows an overall distribution of intermetallic layers in the Inconel regions from sample Multi-Ni-Al 2. Figure 3.3.6-8 sequentially collage the varying elemental distribution of intermetallic layers from the Inconel end to the Al end at higher magnifications. In Figure 3.3.6, the transitional region 1 (thickness ~10 µm), adjacent to Inconel layer, showed a wavy distribution among Ni, Fe and Cr, Mo. In the major intermetallic region 1, one intermetallic phase, $Al_{80}Cr_6Fe_5Ni_8Mo$, was formed uniformly. In the transitional region 2,

it shows that the chemical composition is $Al_{82}Cr_4Fe_3Ni_7Mo$ on average, while in the major region 2 it is $Al_{84}Cr_4Fe_3Ni_7Mo$.

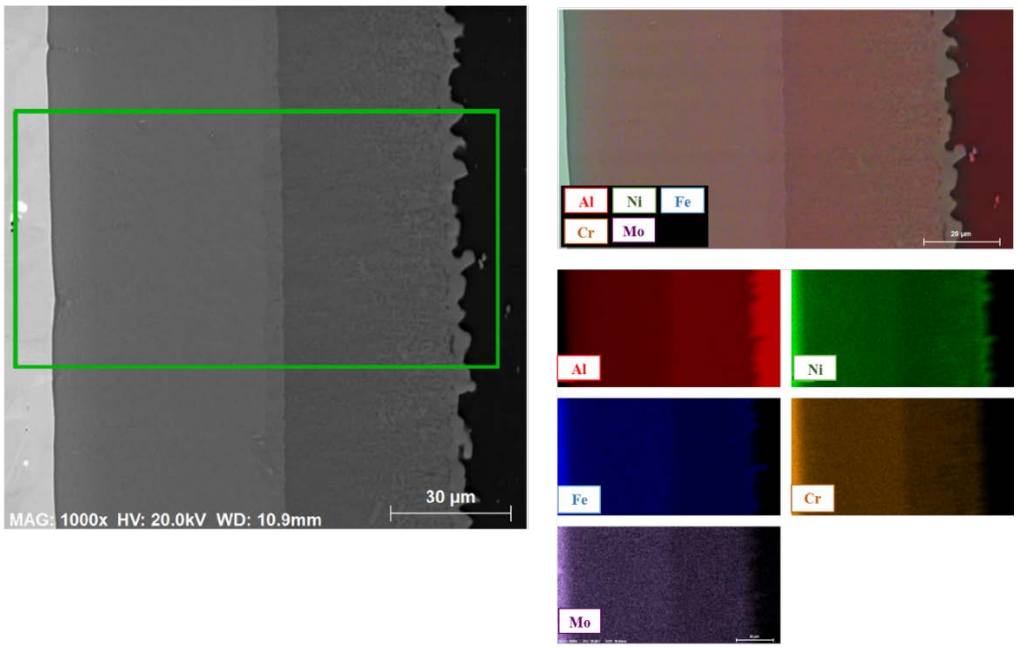

Figure 3.3.5 BSE mapping of intermetallic layers in Inconel regions from sample Multi-Ni-Al 2. MAG: 1000x; HV: 20.0 kV; WD: 10.9mm.

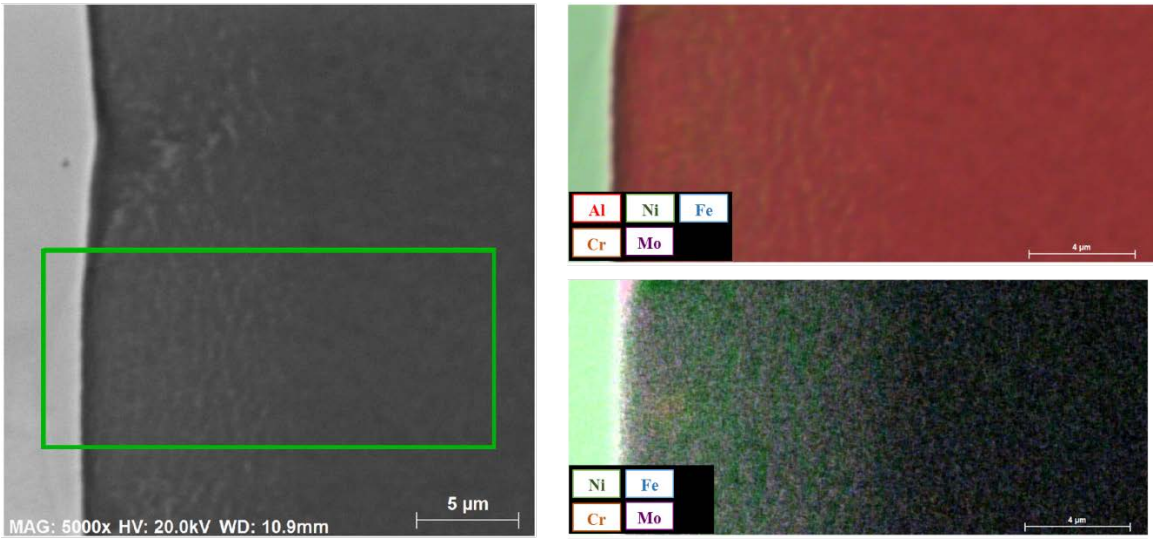

Figure 3.3.6 BSE mapping on the localized region adjacent to Inconel layer. MAG: 5000x; HV: 20.0 kV; WD: 10.9mm.

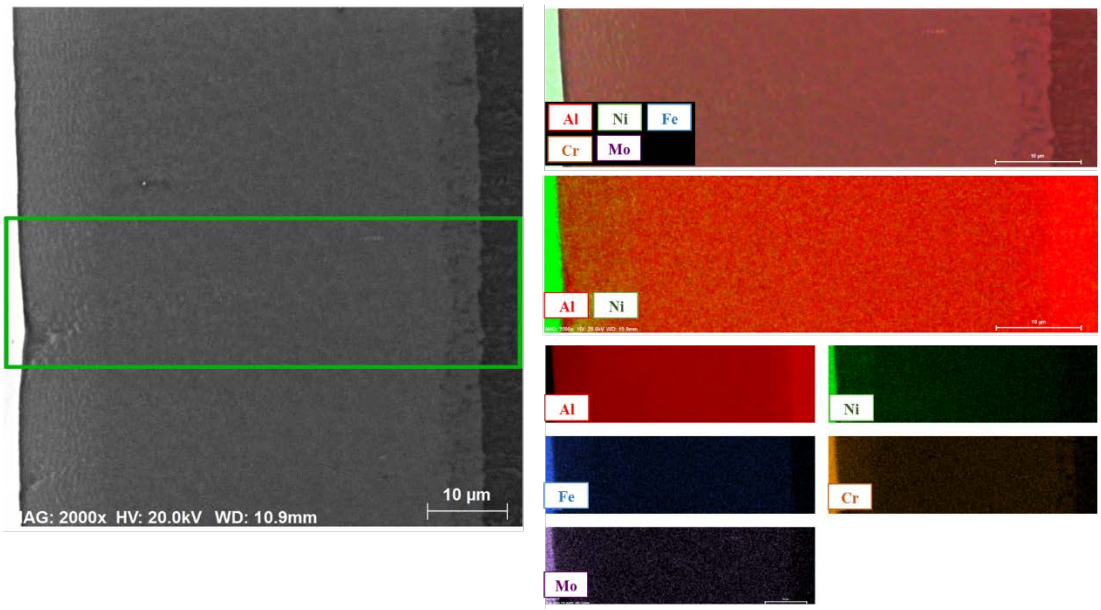

Figure 3.3.7 BSE mapping on the localized region adjacent to Inconel layer at lower magnification. MAG: 2000x; HV: 20.0 kV; WD: 10.9mm.

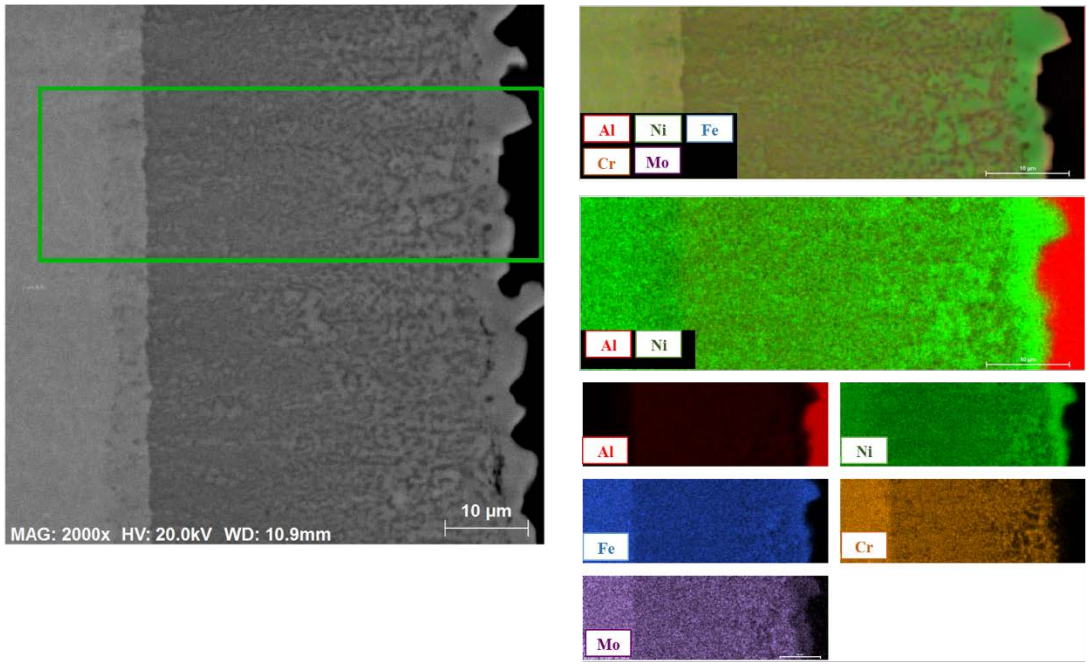

Figure 3.3.8 BSE mapping on the localized region at the front end Inconel layer. MAG: 2000x; HV: 20.0 kV; WD: 10.9mm.

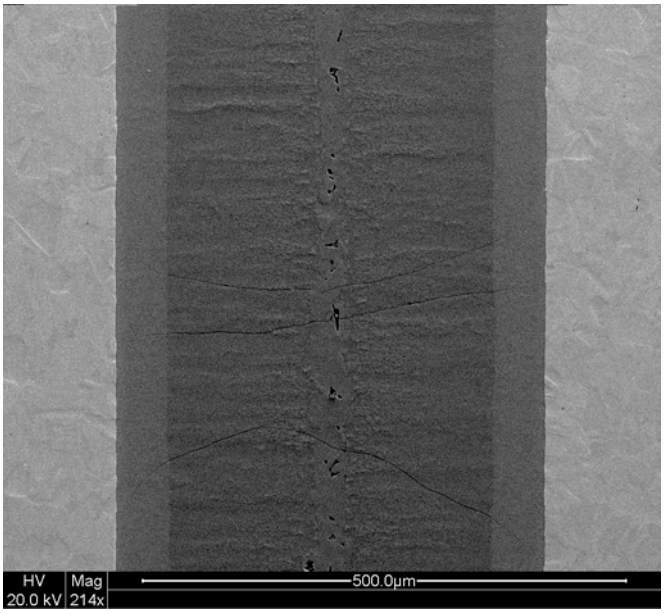

Figure 3.3.9 BSE picture of Inconel regions from sample Multi-Nil-Al 2.

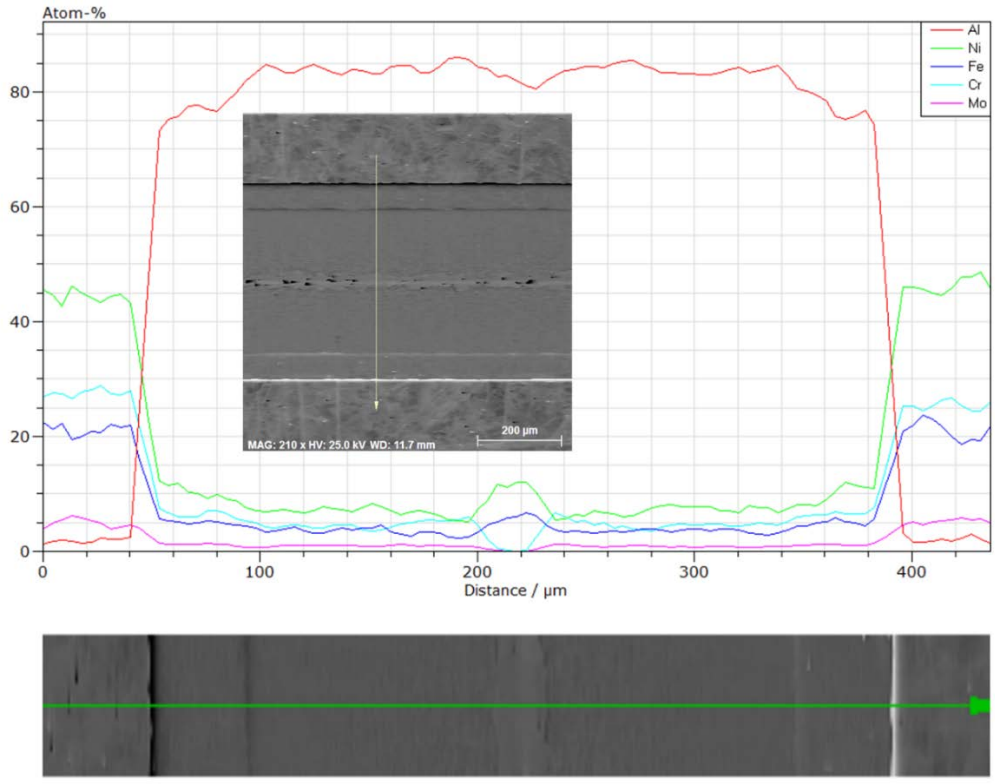

Figure 3.3.10 Linescan over Inconel regions from sample Multi-Ni-Al 2.

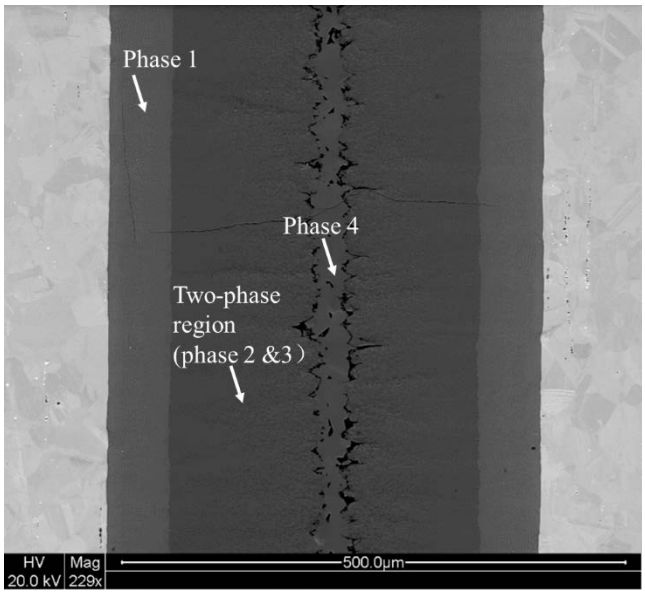

Figure 3.3.11 BSE picture of Inconel regions from sample Multi-Ni-Al-Annealed.

Figure 3.3.7 illustrates that in the annealed Multi-Ni-Al sample, the centerline of $Al_{84}Fe_5Ni_{10}$ was formed between the two-phase intermetallic regions consisting of $Al_{87}Cr_9FeNi_2Mo_2$ and $Al_{85}CrFe_4Ni_9$. The intermetallic layers adjacent to the residual Inconel layers were $Al_{80}Cr_6Fe_5Ni_9Mo$. Phases formed in the Inconel-Al reaction are listed in Table 3.3.1. The chemical compositions obtained in the annealed Multi-Ni-Al sample are in good agreement with compositions obtained in Multi-Ni-Al 2 in which the phases were in developing stage.

Table 3.3.1 Average percentage of elements in Inconel-Al-based composite layer

Phase #	Chemical Compositions (at%)				
	Al (at%)	Cr (at%)	Fe (at%)	Ni (at%)	Mo (at%)
Phase 1	80	6	5	9	1
Phase 2 (In two-phase region)	87	9	1	2	2
Phase 3 (In two-phase region)	85	1	4	10	0
Phase 4 (Centerline)	84	0	5	10	0

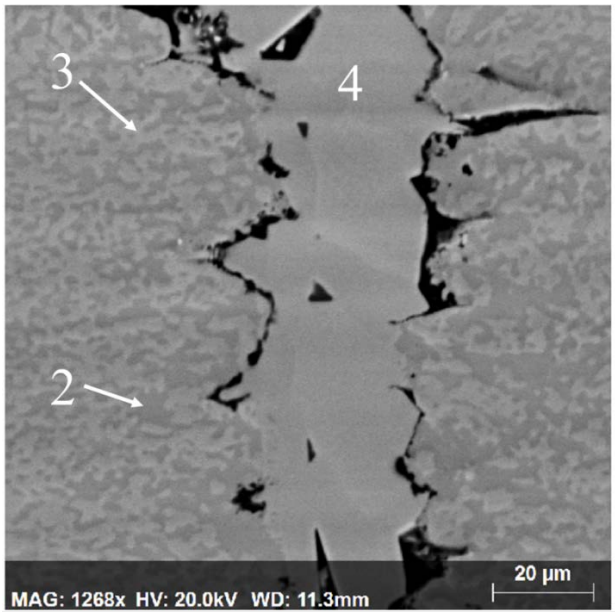

Figure 3.3.12 BSE picture showing phases 2, 3 and 4 in the center layer in Inconel-Al region from sample Multi-Ni-Al-Annealed.

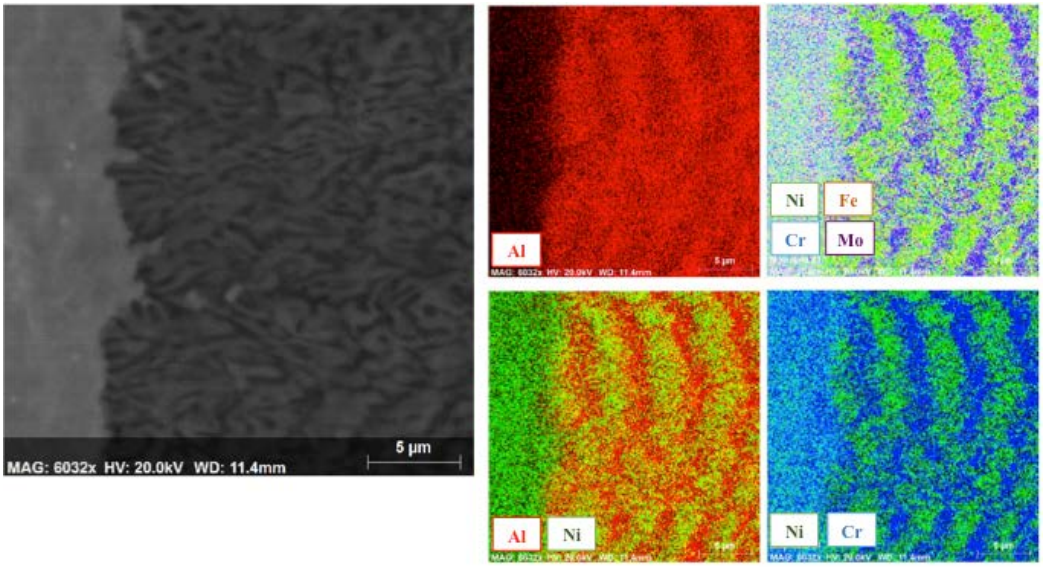

Figure 3.3.13 The multipoints and mapping scans shows a wave-like distribution. MAG: 6032x HV: 20.0 kV WD: 11.4mm

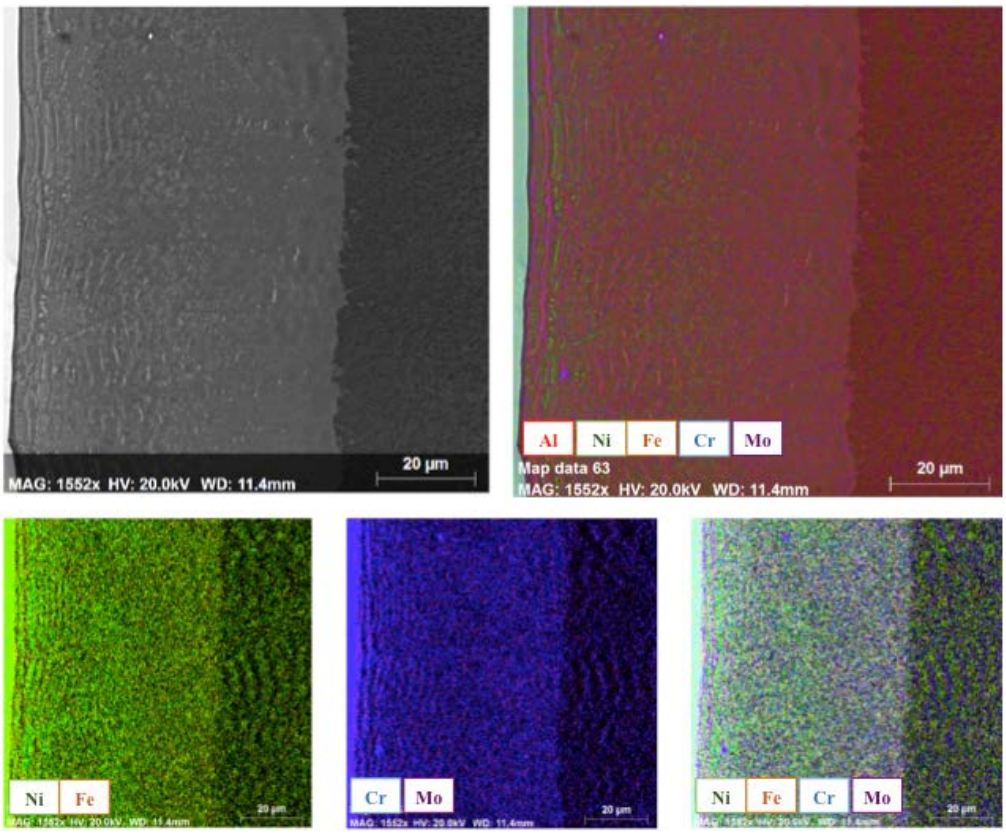

Figure 3.3.14 The mapping scan over $Al_{80}Cr_6Fe_5Ni_9Mo$ layer and two-phase layer. MAG: 1552x HV: 20.0 kV WD: 11.4mm

As shown in Figure 3.3.8 and Figure 3.3.9, a wave-like distribution among Ni, Fe, Cr and Mo exists throughout the intermetallic layers. This may be caused by the difference in diffusion rates of the studied elements. According to the equation

$$\mathrm{D} = D_0 \exp(-\frac{Q_d}{RT})$$

where

D_0 = a temperature-independent preexponential (m^2/s)

Q_d = the activation energy for diffusion (J/mol)

R = the gas constant, 8.31 J/mol·K

T = absolute temperature (K)

Diffusion coefficients for Ni, Fe, Cr, and Mo in Al at 923 K (650℃) were calculated as listed in Table 3.3.2.

As an indicator of the diffusion rates, the difference in magnitudes of the diffusion coefficient D among Ni, Fe, Cr, and Mo, shows that Ni and Fe are the two diffusing species which have much higher diffusion rates in Al than Cr and Mo. When the reaction first begins, as the compositional gradient is the driving force, higher diffusion rates of Ni and Fe promote their reaction with Al predominantly, forming phases richer in Ni and Fe. Such consumption of Ni and Fe generates a layer which has higher contents of Cr and Mo, hence as the front Ni-Fe-rich layer is formed, it is followed by a layer that has higher Cr and Mo instead, which then reacts with Al. As the surplus of Cr and Mo is consumed forming a Cr-Mo-rich layer following the Ni-Fe-rich layer, the predominant reaction goes back to the prior situation where Ni and Fe are the major species to react with Al. This cycle of reaction generates a wave-like distribution among Ni, Fe and Cr, Mo, as can been seen from Figure 3.3.8 and Figure 3.3.9. Figure 3.3.15 shows a mapping result on composition distribution over the intermetallic regions, with red represent Al, green for Ni, orange for Cr, blue for Fe and purple for Mo. The centerline shows a deficiency of Cr and Mo.

Table 3.3.2 A Tabulation of Diffusion Data with Aluminum as Host Metal [13]

Diffusing species	D_0 (cm^2/s)	Activation energy Q_d (kJ/mol)	Temp. range (K)	Calculated D at 923 K (m^2/s)
Ni	4.4	145.8	742-924	2.44×10^{-12}
Fe	53	183.4	793-930	2.19×10^{-13}
Cr	1.85×10^{3}	253	859-923	8.74×10^{-16}
Mo	14	250	898-928	9.78×10^{-18}

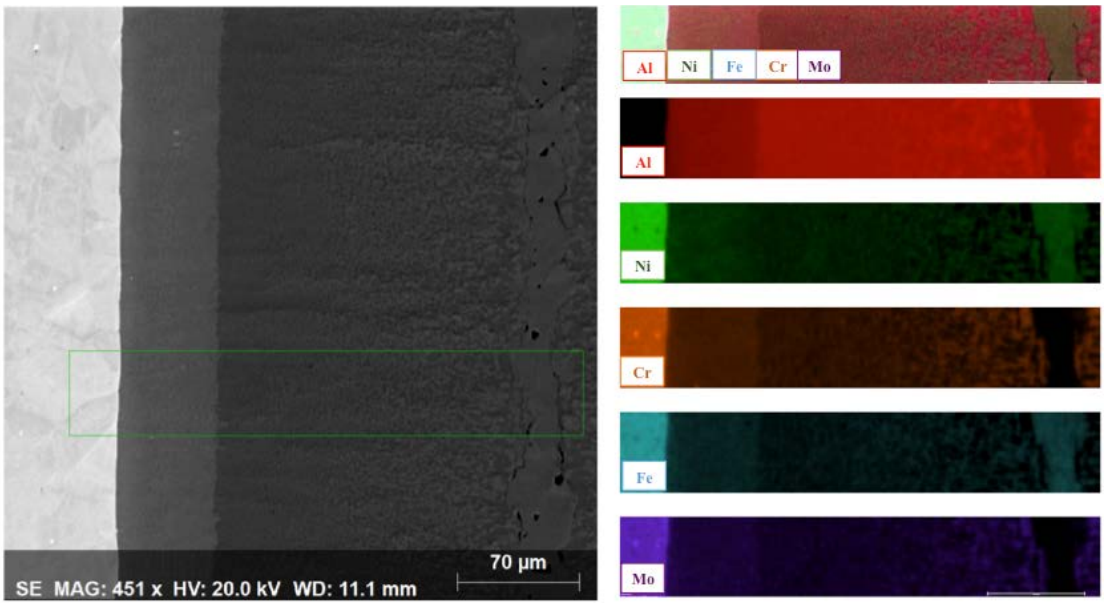

Figure 3.3.15 The mapping scan across the intermetallic layers in the Inconel regions from sample Multi-Ni-Al 2. MAG: 451x HV: 20.0 kV WD: 11.1mm

3.3.2 Nano-Indentation Tests for Inconel-Al

The testing method was the same as the pure nickel sample tests. For each set of indentation tests, in every morphologically distinctive layer, a matrix of 5 x 10 indentation locations were selected with an indent distance of 80 µm. Among the 10 tested sets, 4 sets were located in the Inconel layers, 2 sets in the $Al_{80}Cr_6Fe_5Ni_9Mo$ layers, and 4 sets in the two-phase layers from both sides.

As can be seen from Graph 3.2.1, the moduli show an inconsistency over the two-phase intermetallic regions after heat treatment. This may be caused by the indentation on grains of different intermetallic phases. In spite of the inconsistency, modulus in the two-phase regions with an average value of 158.3 GPa, shows a slight decrease comparing to that of Inconel layer, with an average value of 162.1 GPa, while $Al_{80}Cr_6Fe_5Ni_9Mo$ intermetallic layers have an increase of 5 GPa.

However, from Graph 3.3.2, the hardness results were consistent, showing a significant increase between the intermetallic regions and unreacted Inconel layers. A

symmetric tendency confirms that the reaction from both sides are consistent. In Table 3.3.3, averaged values of modulus and hardness were listed.

Table 3.3.3 Modulus and hardness results obtained on Inconel and intermetallics

	Modulus/GPa	Hardness/GPa
Inconel	162.1	2.5
$Al_{80}Cr_6Fe_5Ni_9Mo$ layers	167.1	8.7
Two-phase regions	158.3	6.8

Graph 3.3.1 The transition of modulus at maximum load in Inconel-Al sample.

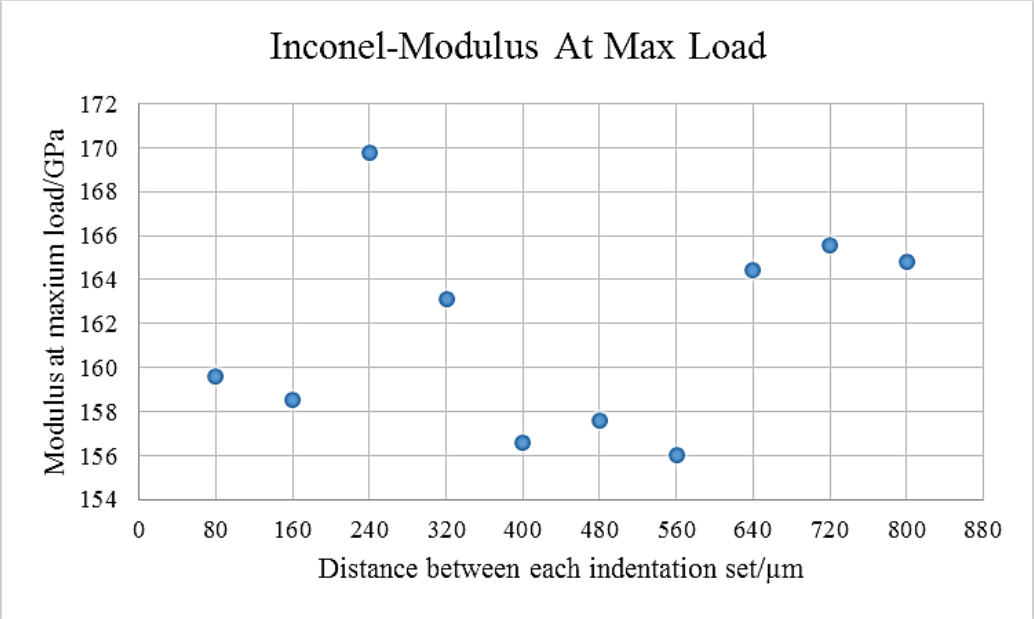

Graph 3.3.2 The transition of hardness at maximum load in Inconel-Al sample.

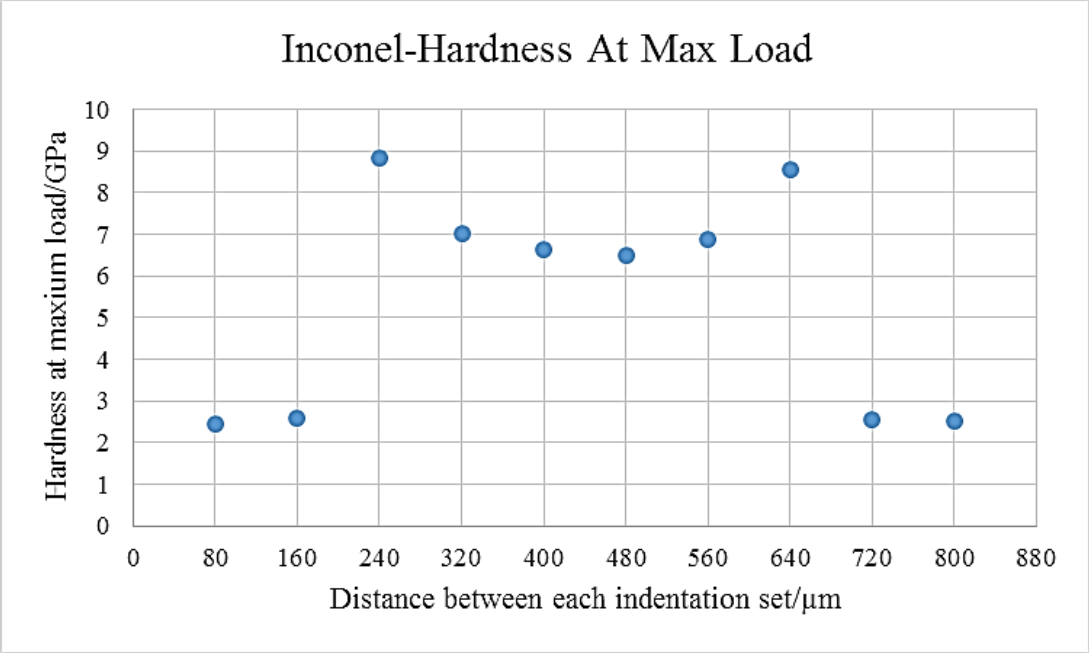

CHAPTER 4: CONCLUSIONS

Under the heat processing methods described in Chapter 2, several samples were made which investigated the reactions between aluminum and pure nickel, Invar, and Inconel respectively. From the binary phase diagram of Ni and Al, the eutectic temperature between Ni and Al is around 640℃. Two phases formed were Al_3Ni_2 and Al_3Ni. The nanoindentation tests showed that the values of modulus at maximum load in the intermetallic layers were slightly increased comparing to the rest pure Ni layers, while average value of the hardness was around ten times of the one in the residual pure Ni layer. In the reaction between Invar and aluminum, two major intermetallic phases, $Al_{79}Fe_{16}Ni_6$ and $Al_{84}Fe_9Ni_7$ were obtained. The intermetallic layer of $Al_{80}Cr_6Fe_5Ni_9Mo$, and the two-phase layer of $Al_{87}Cr_9FeNi_2Mo_2$ and $Al_{85}CrFe_4Ni_9$ were obtained from the reaction between Inconel and aluminum. At 635℃ the average lengths of total intermetallic layers in Inconel was comparable to those in pure Ni-Al, while the lengths in Invar indicated a slower growth rate comparing to pure Ni and Inconel reactions.

The main conclusions are as follow:

1. Under the given heat processing, for binary nickel-aluminum system, the reaction evolution goes through four major stages. Stage 1 is featured with the formation of Al_3Ni_2 nodules at the interface between nickel and aluminum foils. In stage 2, as temperature reaches the melting point of Al, while nodules of Al_3Ni_2 grow larger and merge into layers, the second intermetallic Al_3Ni starts to form at the front of Al_3Ni_2 layer. In stage 3 of intermetallic layer expansion, both layers of intermetallic phases continue to advance into the center of Al layer. In the final stage where original Al layer is fully consumed, two major intermetallic phases, Al_3Ni_2 and Al_3Ni occupy where the original Al layer is.

2. Once the temperature reaches the melting point of Al, the occurrence of solid-liquid reaction between Ni and liquid Al will further accelerate the formation of both intermetallic phases.

3. Fe in the aluminum foils will react and form a thin layer of $Al_{80}Fe_5Ni_{15}$ in the center of reacted intermetallic layers.

4. Young's modulus in Al_3Ni_2 layers has an average value of 157.8 GPa and hardness of 4.2 GPa, while the modulus of Al_3Ni has an average value of 188.9 GPa and hardness of 9.7 GPa. Comparing to the modulus (126.9 GPa) and hardness (1.2GPa) in residual nickel layer, both modulus and hardness have been significantly improved over the intermetallic areas in the composite.

5. For ternary nickel-iron-aluminum system, at the beginning of reaction nodules of $Al_{75}Fe_{20}Ni_{15}$ first formed at the interface. The reaction continues and then forms a thin layer of $Al_{80}Fe_{15}Ni_5$.

6. In the annealed sample, an intermetallic layer of $Al_{79}Fe_{16}Ni_6$ was formed by the side of Invar layer, and a two-phase layer of $Al_{79}Fe_{16}Ni_6$ and $Al_{84}Fe_9Ni_7$ were formed following the $Al_{79}Fe_{16}Ni_6$ layer.

7. From the anneal multi-Ni-Al sample, a Ni-rich centerline consisting of $Al_{84}Fe_9Ni_7$ was found, while the cause for the generation of cavities in the center may be the deletion of Al and Ni atoms, since as the reaction proceeds, the richer Fe content promotes the formation of more $Al_{79}Fe_{16}Ni_6$.

8. Young's modulus in Invar layers after heat processing has an average value of 117.8 GPa and hardness of 1.52 GPa, while the modulus of two-phase intermetallic layer has an average value of 154.0 GPa and hardness of 7.5 GPa. The centerline of $Al_{84}Fe_9Ni_7$ has a modulus of 120.3 GPa, and hardness of 4.6 GPa.

9. For nickel-chromium-iron-molybdenum-aluminum system, the intermetallic layer of $Al_{80}Cr_6Fe_5Ni_9Mo$ was formed near to the Inconel side, which was

followed by a two-phase layer of $Al_{87}Cr_9FeNi_2Mo_2$ and $Al_{85}CrFe_4Ni_9$ and a centerline of $Al_{84}Fe_5Ni_{10}$ which contained no trace of Cr nor Mo.

10. As listed in Table 3.3.2, Ni and Fe have much higher diffusion rates in Al than Cr and Mo. According to the Kirkendall effect, such difference in diffusion rates leads to a wave-like distribution among Ni, Fe and Cr, Mo. Driven by compositional gradients, higher diffusion rates of Ni and Fe promote their reaction with Al predominantly, forming phases richer in Ni and Fe. While the consumption of Ni and Fe continues, it leaves a layer with higher contents of Cr and Mo behind, which then reacts with upcoming Al. As Cr and Mo are consumed forming Cr-Mo-rich phases, the predominant reaction goes back to the prior situation where Ni and Fe are the major species to react with Al. Such reaction cycle then lead to the wave-like distribution among the elements.

11. Young's modulus in Inconel layers has an average value of 162.1 GPa and hardness of 2.5 GPa, while the modulus of $Al_{80}Cr_6Fe_5Ni_9Mo$ layer has an average value of 167.1 GPa and hardness of 8.7 GPa. The two-phase layer of $Al_{87}Cr_9FeNi_2Mo_2$ and $Al_{85}CrFe_4Ni_9$ has a modulus of 158.3 GPa, and hardness of 6.8 GPa.

REFERENCES

[1] Stoloff, N. S., C. T. Liu, and S. C. Deevi. "Emerging applications of intermetallics." Intermetallics 8.9 (2000): 1313-1320.

[2] Koch, Carl C., and J. D. Whittenberger. "Mechanical milling/alloying of intermetallics." *Intermetallics* 4.5 (1996): 339-355.

[3] Deevi, S. C., and V. K. Sikka. "Nickel and iron aluminides: an overview on properties, processing, and applications." *Intermetallics* 4.5 (1996): 357-375.

[4] Deevi, S. C., V. K. Sikka, and C. T. Liu. "Processing, properties, and applications of nickel and iron aluminides." *Progress in Materials Science* 42.1 (1997): 177-192.

[5] Vecchio, Kenneth S. "Synthetic multifunctional metallic-intermetallic laminate composites." Jom 57.3 (2005): 25-31.

[6] Harach, David J., and Kenneth S. Vecchio. "Microstructure evolution in metal-intermetallic laminate (MIL) composites synthesized by reactive foil sintering in air." Metallurgical and Materials Transactions A 32.6 (2001): 1493-1505.

[7] Polmear, Ian. Light alloys: from traditional alloys to nanocrystals. Butterworth-Heinemann, 2005.

[8] Rohatgi, Aashish, et al. "Resistance-curve and fracture behavior of Ti–Al_3Ti metallic–intermetallic laminate (MIL) composites." *Acta Materialia* 51.10 (2003): 2933-2957.

[9] Konieczny, M. "Microstructural characterisation and mechanical response of laminated Ni-intermetallic composites synthesised using Ni sheets and Al foils." Materials Characterization 70 (2012): 117-124.

[10] Kattner, Ursula R. "The thermodynamic modeling of multicomponent phase equilibria." JOM 49.12 (1997): 14-19.

[11] Betteridge, W. *Nickel and Its Alloys*. Chichester, West Sussex, England: Ellis Horwood ;, 1984. Print.

[12] Heubner, Ulrich. *Nickel Alloys*. New York: Marcel Dekker, 1998. Print.

[13] Dongmin Shi, Bin Wen, Roderick Melnik, Shan Yao, Tingju Li, First-principles studies of Al–Ni intermetallic compounds, Journal of Solid State Chemistry, Volume 182, Issue 10, October 2009, Pages 2664-2669, ISSN 0022-4596.

[14] Smithells, Colin J., and W. F. Gale. *Smithells Metals Reference Book*. 8th Ed. / ed. Amsterdam: Elsevier Butterworth-Heinemann, 2004. Print.